Article

A Biomimetic Approach to Oxidized Sites in the Xanthine Oxidoreductase Family: Synthesis and Stereochemistry of Tungsten(VI) Analogue Complexes

Stanislav Groysman, Jun-Jieh Wang, Ranitendranath Tagore, Sonny C. Lee, and R. H. Holm

J. Am. Chem. Soc., **2008**, 130 (38), 12794-12807 • DOI: 10.1021/ja804000k • Publication Date (Web): 03 September 2008

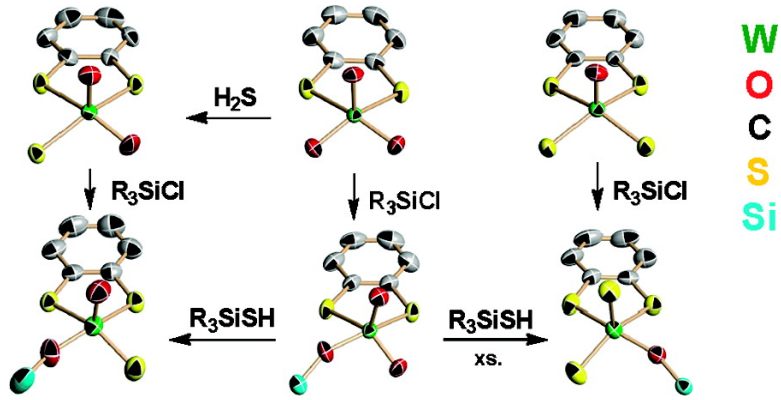

More About This Article

Additional resources and features associated with this article are available within the HTML version:

- Supporting Information
- Links to the 1 articles that cite this article, as of the time of this article download
- Access to high resolution figures
- Links to articles and content related to this article
- Copyright permission to reproduce figures and/or text from this article

View the Full Text HTML

J|A|C|S
ARTICLES

Published on Web 09/03/2008

A Biomimetic Approach to Oxidized Sites in the Xanthine Oxidoreductase Family: Synthesis and Stereochemistry of Tungsten(VI) Analogue Complexes

Stanislav Groysman,† Jun-Jieh Wang,† Ranitendranath Tagore,† Sonny C. Lee,*,‡ and R. H. Holm*,†

Department of Chemistry and Chemical Biology, Harvard University, Cambridge, Massachusetts 02138, and Department of Chemistry, University of Waterloo, Waterloo, Ontario, Canada N2L 3G1

Received May 28, 2008; E-mail: sclee@uwaterloo.ca; holm@chemistry.harvard.edu

Abstract: Two series of square pyramidal (SP) monodithiolene complexes, $[M^{VI}O_{3-n}S_n(bdt)]^{2-}$ and their silylated derivatives $[M^{VI}O_{2-n}S_n(OSiR_3)(bdt)]^-$ ($n = 0$, M = Mo or W; $n = 1$, 2, M = W), synthesized in this and previous work, constitute the basic molecules in a biomimetic approach to structural analogues of the oxidized sites in the xanthine oxidoreductase enzyme family. Benzene-1,2-dithiolate (bdt) simulates native pyranopterindithiolene chelation in the basal plane, tungsten instead of the native metal molybdenum was employed in sulfido complexes to avoid autoreduction, and silylation models protonation. The complexes $[MO_3(bdt)]^{2-}$ and $[MO_2(OSiR_3)(bdt)]^-$ represent inactive sites, while $[MO_2S(bdt)]^{2-}$ and $[MOS(OSiR_3)(bdt)]^-$, with basal sulfido and silyloxo ligands, are the first analogues of the catalytic sites. Also prepared were $[MOS_2(bdt)]^{2-}$ and $[MS_2(OSiR_3)(bdt)]^-$, with basal sulfido and silyloxo ligands. Complexes are described by angular parameters which reveal occasional distortions from idealized SP toward a trigonal bipyramidal (TBP) structure arising from crystal packing forces in crystalline Et_4N^+ salts. Miminized energy structures from DFT calculations are uniformly SP and reproduce experimental structures. For example, the correct structure is predicted for $[WO_2S(bdt)]^{2-}$, whose basal and apical sulfido diastereomers are potentially interconvertible through a low-lying TBP transition state for pseudorotation. The lowest energy tautomer of the protonated form is calculated to be $[WOS(OH)(bdt)]^-$, with basal sulfido and hydroxo ligands. Computational and experimental structures indicate that protein sites adopt intrinsic coordination geometries rather than those dictated by protein structure and environment.

Introduction

We seek accurate synthetic analogues of the mononuclear active sites of molybdenum- and tungsten-containing enzymes[1−7] in order to reveal intrinsic structural and electronic features of these sites while disclosing heretofore unexplored fundamental chemistry of the native metals. The large majority of our research has been directed at analogues of sites in the dimethylsulfoxide reductase (DMSOR) family of enzymes,[1] which in the oxidized state contain a Mo^{VI} atom coordinated by two pyranopterindithiolene, one oxo/hydroxo, and one protein-based ligand(s). Structural and functional analogues based on dithiolene coordination have been developed and are summarized elsewhere,[8] with the most recent analogue systems relevant to selenate reductase[9] and formate dehydrogenase.[10] The sulfite oxidase and xanthine oxidoreductase (XOR) molybdoenzyme families differ from the DMSOR[11] family by implicating *one* pyranopterindithiolene chelate ligand. The XOR family, whose most prominent members are xanthine oxidoreductase itself and aldehyde oxidoreductase (AOR), is differentiated in part from the sulfite oxidase family by the oxidized active site composition $\{Mo^{VI}(S_2pd)O_2S\}$, in which one oxo ligand may be protonated, compared to $\{Mo^{VI}(S_2pd)O_2(S_{Cys})\}$. Active sites in the XOR family include a sulfido but no protein-based ligand. The terminal sulfido ligand is essential for enzymatic activity in the hydroxylation of C−H bonds in purines and related substrates ($RH + H_2O \rightarrow ROH + 2H^+ + 2e^-$) and in the oxidation of aldehydes to acids ($RCHO + H_2O \rightarrow RCOOH + 2H^+ + 2e^-$).[1,6,7]

Known active site structures in the XOR family are schematically depicted in Figure 1. Crystallographic refinement of inactive *Desulfovibrio gigas* AOR at 1.28 Å resolution reveals the indicated square pyramidal (SP) stereochemistry, with a

† Harvard University.
‡ University of Waterloo.

(1) Hille, R. *Chem. Rev.* **1996**, *96*, 2757–2816.
(2) Johnson, M. K.; Rees, D. C.; Adams, M. W. W. *Chem. Rev.* **1996**, *96*, 2817–2839.
(3) Kisker, C.; Schindelin, H.; Rees, D. C. *Annu. Rev. Biochem.* **1997**, *66*, 233–267.
(4) Schindelin, H.; Kisker, C.; Rajagopalan, K. V. *Adv. Protein Chem.* **2001**, *58*, 47–94.
(5) Hille, R. *Trends Biochem. Sci.* **2002**, *27*, 360–367.
(6) Hille, R. *Arch. Biochem. Biophys.* **2005**, *433*, 107–116.
(7) Hille, R. *Eur. J. Inorg. Chem.* **2006**, 1913–1926.
(8) Enemark, J. H.; Cooney, J. J. A.; Wang, J.-J.; Holm, R. H. *Chem. Rev.* **2004**, *104*, 1175–1200.
(9) Wang, J.-J.; Tessier, C.; Holm, R. H. *Inorg. Chem.* **2006**, *45*, 2979–2988.
(10) Groysman, S.; Holm, R. H. *Inorg. Chem.* **2007**, *46*, 4090–4102.
(11) Abbreviations are summarized in Chart 1.

10.1021/ja804000k CCC: $40.75

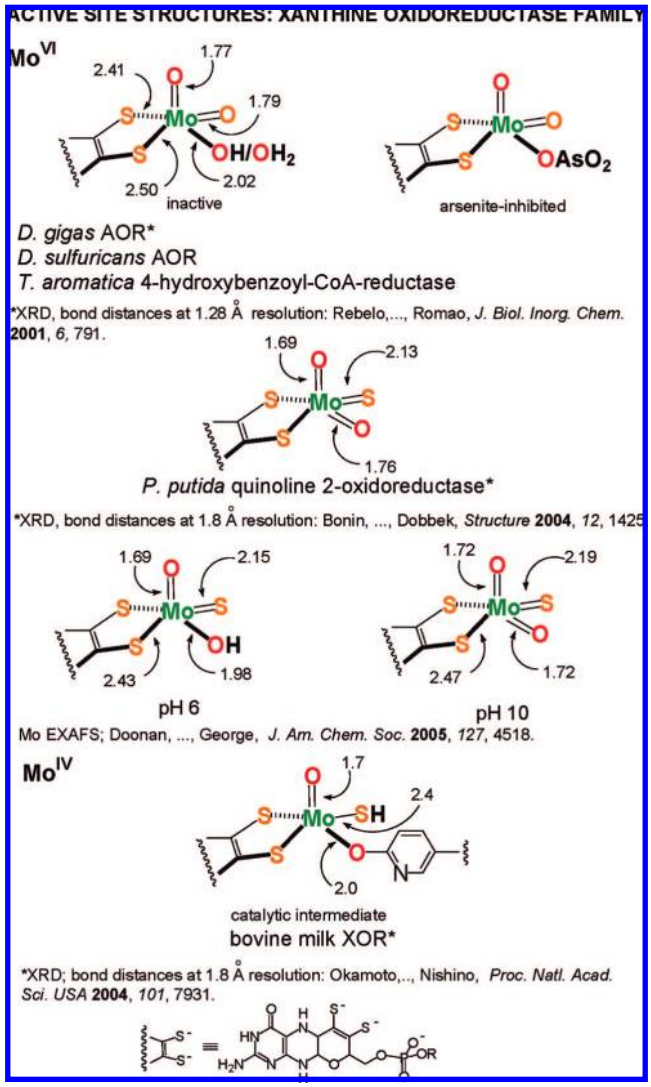

Figure 1. Schematic representations of active site structures in the xanthine oxidoreductase enzyme family, including available bond distances (Å).

reported aquo ligand in a basal position and oxo ligands in apical and basal locations.[12] A similar structure has been assigned or modeled to the inactive forms of *Desulfovibrio desulfuricans* AOR[13] and *Thauera aromatica* 4-hydroxybenzoyl-CoA-reductase,[14] with either water or hydroxo as a basal ligand. In the case of arsenite-inhibited *D. gigas* AOR, arsenite occupies this position.[15] In active enzymes, the sulfido ligand was assigned to the apical position from an X-ray structure of oxidized, resulfidated *D. gigas* AOR.[16] This structure was also applied to the oxidized sites of bovine milk xanthine oxidase/xanthine dehydrogenase (XO/XDH)[17] and *Rhodobacter capsulatus* XDH,[18] for which the X-ray data did not allow direct identification of all molybdenum ligands. Subsequently, however, the X-ray structure of native *Pseudomonas putida* quinoline 2-oxidoreductase (QOR) demonstrated that the sulfido ligand occupies a *basal* position, with a Mo^{VI}=S bond distance of 2.13 Å.[19] Molybdenum extended X-ray absorption fine structure (EXAFS) analysis of bovine XO has yielded accurate bond distances and demonstrated a marked contraction of one Mo−O bond at pH 10 vs pH 6, consistent with a terminal hydroxo-to-oxo conversion.[20] The X-ray structure of a catalytic intermediate of milk XO discloses a basal hydrosulfide ligand with a Mo−S bond distance of 2.4 Å. Consequently, the sites $\{Mo^{VI}(S_2pd)O_2S\}$/$\{Mo^{VI}(S_2pd)O(OH/OH_2)S\}$, related by protonation, now appear to be adequately established.

Our initial attempts to prepare dithiolene analogues of sites in the XO enzyme family afforded SP $[MO_3(bdt)]^{2-}$ (M = Mo, W)[21] by the procedure in Figure 2. These complexes are viable structural analogues of unprotonated inactive oxidized sites and serve as precursors for other molecules of pertinence to the XO site problem. For example, they can be converted to $[MO_2(OSiR_3)(bdt)]^-$,[21,22] in which the silyloxo ligand occupies a basal position, as does hydroxo in enzyme sites. For structural purposes in this and other cases (vide infra), silylation simulates protonation. Achievement of an active site analogue necessitates the introduction of a sulfido ligand. The cisoid group $M^{VI}OS$ has been stabilized in complexes (excluding organometallics) with M = Mo[23−26] and W.[27−32] While these species are of considerable interest in their own right, they are usually six-coordinate and do not contain a dithiolene ligand which would model the structural and electronic features of the pyranopterindithiolene cofactor ligand in an enzyme site.

Recently, we have reported the first structural analogue of an oxidized site in the XOR family. The complex $[WO_2S(bdt)]^{2-}$ has the desired SP stereochemistry, with an apical oxo ligand and basal oxo, sulfido, and dithiolene ligands.[33] In this report, we provide a full account of the synthesis and structural properties of molecules in the series $[W^{VI}O_{3-n}S_n(bdt)]^{2-}$ (n = 0−2) and $[W^{VI}O_{2-n}S_n(OSiR_3)(bdt)]^-$ (n = 1, 2), including a density functional theory (DFT) treatment of stereochemistry.

(12) Rebelo, J. M.; Dias, J. M.; Huber, R.; Moura, J. J. G.; Romão, M. J. *J. Biol. Inorg. Chem.* **2001**, *6*, 791–800.
(13) Rebelo, J.; Maceira, S.; Dias, J. M.; Huber, R.; Ascenso, C. S.; Rusnak, F.; Moura, J. J. G.; Moura, I.; Romão, M. J. *J. Mol. Biol.* **2000**, *297*, 135–146.
(14) Unciuleac, M.; Warkentin, E.; Page, C. C.; Boll, M.; Ermler, U. *Structure* **2004**, *12*, 2249–2256.
(15) Boer, D. R.; Thapper, A.; Brondino, C. D.; Romão, M. J.; Moura, J. J. G. *J. Am. Chem. Soc.* **2004**, *126*, 8614–8615.
(16) Huber, R.; Hof, P.; Duarte, R. O.; Moura, J. J. G.; Moura, I.; Liu, M.-Y.; LeGall, J.; Hille, R.; Archer, M.; Romão, M. J. *Proc. Natl. Acad. Sci. U.S.A.* **1996**, *93*, 8846–8851.
(17) Enroth, C.; Eger, B. T.; Okamoto, K.; Nishino, T.; Nishino, T.; Pai, E. F. *Proc. Natl. Acad. Sci. U.S.A.* **2000**, *97*, 10723–10728.
(18) Truglio, J. J.; Theis, K.; Liemkühler, S.; Rappa, R.; Rajagopalan, K. V.; Kisker, C. *Structure* **2002**, *10*, 115–125.
(19) Bonin, I.; Martins, B. M.; Purvanov, V.; Fetzner, S.; Huber, R.; Dobbek, H. *Structure* **2004**, *12*, 1425–1435.
(20) Doonan, C. J.; Stockert, A.; Hille, R.; George, G. N. *J. Am. Chem. Soc.* **2005**, *127*, 4518–4522.
(21) Partyka, D. V.; Holm, R. H. *Inorg. Chem.* **2004**, *43*, 8609–8616.
(22) Wang, J.-J.; Holm, R. H. *Inorg. Chem.* **2007**, *46*, 11156–11164.
(23) Eagle, A. A.; Laughlin, L. J.; Young, C. G.; Tiekink, E. R. T. *J. Am. Chem. Soc.* **1992**, *114*, 9195–9197.
(24) Thapper, A.; Donahue, J. P.; Musgrave, K. B.; Willer, M. W.; Nordlander, E.; Hedman, B.; Hodgson, K. O.; Holm, R. H. *Inorg. Chem.* **1999**, *38*, 4104–4114.
(25) Doonan, C. J.; Nielson, D. J.; Smith, P. D.; White, J. M.; George, G. N.; Young, C. G. *J. Am. Chem. Soc.* **2006**, *128*, 305–316.
(26) Laughlin, L. J.; Eagle, A. A.; George, G. N.; Tiekink, E. R. T.; Young, C. G. *Inorg. Chem.* **2007**, *46*, 939–948.
(27) Wollert, R.; Rentschler, E.; Massa, W.; Dehnicke, K. *Z. Anorg. Allg. Chem.* **1991**, *596*, 121–132.
(28) Potvin, C.; Manoli, J. M.; Marzak, S.; Secheresse, F. *Acta Crystallogr.* **1988**, *C44*, 369–370.
(29) Eagle, A. A.; Harben, S. M.; Tiekink, E. R. T.; Young, C. G. *J. Am. Chem. Soc.* **1994**, *116*, 9749–9750.
(30) Miao, M.; Willer, M. W.; Holm, R. H. *Inorg. Chem.* **2000**, *39*, 2843–2849.
(31) Eagle, A. A.; Tiekink, E. R. T.; George, G. N.; Young, C. G. *Inorg. Chem.* **2001**, *40*, 4563–4573.
(32) Thomas, S.; Eagle, A. A.; Sproules, S. A.; Hill, J. P.; White, J. M.; Tiekink, E. R. T.; George, G. N.; Young, C. G. *Inorg. Chem.* **2003**, *42*, 5909–5916.

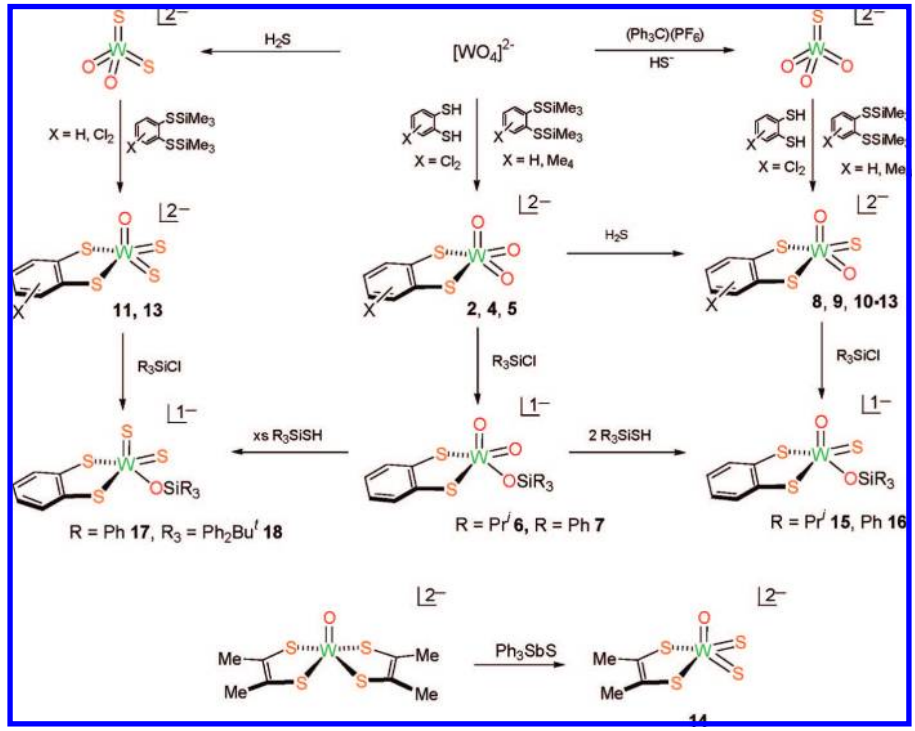

Figure 2. Synthesis of oxo/sulfido-dithiolene W^{VI} complexes **8**−**14** and monosilylated derivatives **15**−**18** in acetonitrile or acetonitrile/THF solutions by sulfidation or silylation reactions. Preparations of precursor anions $[WO_{4-n}S_n]^{2-}$ ($n = 1$,[21] 2[40]) and oxo-silyloxide complexes **6** and **7**[21,22] have been previously reported.

Throughout, tungsten is used in place of molybdenum without compromise of structural fidelity. Isoelectronic Mo^{VI} and W^{VI} molecules with the same ligands are always isostructural and practically isometric. However, at parity of ligation, Mo^{VI} is more easily reduced, leading to an inability to prepare certain Mo^{VI} complexes whose W^{VI} counterparts are stable. This situation is exacerbated in an anionic sulfur ligand environment.[8,34] We have recently utilized tungsten complexes in the development of functional analogue systems of nitrate reductase,[35] selenate reductase,[9] and structural analogues of formate dehydrogenase sites.[10]

Experimental Section

Preparation of Compounds. All reactions and manipulations were performed under a pure dinitrogen atmosphere using either an inert atmosphere box or standard Schlenk techniques. Acetonitrile, diethyl ether, and tetrahydrofuran (THF) were freshly purified using an Innovative Technology or MBraun solvent purification system and stored over 4-Å molecular sieves. Benzene-1,2-dithiol (H_2(bdt)) was prepared by a literature method.[36] All volume reduction and drying steps were carried out in vacuo. IR spectra were recorded in KBr pellets and absorption spectra in acetonitrile solutions. ^{1}H NMR data for tungsten compounds refer to anions in CD_3CN solutions. Compounds were characterized by ^{1}H NMR, IR, and mass spectra and, for selected compounds, by elemental analysis (H. Kolbe, Mulheim, Germany) and X-ray crystal structure determinations. Electrospray mass spectra of most tungsten compounds reveal a prominent peak for the parent ion (M^-).

Bis(1,2-trimethylsilylthio)benzene. This convenient preparation was adopted from a published procedure.[37] Triethylamine (4.04 g, 40.0 mmol) was added dropwise to a solution of 2.84 g (20.0 mmol) of H_2(bdt) in 100 mL of hexanes at 0 °C, immediately producing a white precipitate. The reaction mixture was stirred for 5 min, 4.34 g (40.0 mmol) of Me_3SiCl was added, and stirring was continued overnight. The mixture was filtered and solvent removed from the filtrate, leaving the product as 5.09 g (89%) of colorless liquid. ^{1}H NMR: δ 0.29 (s, 18), 7.19 (dd, 2), 7.53 (dd, 2).

Bis(1,2-trimethylsilylthio)tetramethylbenzene. To a solution of 330 mg (1.67 mmol) of tetramethylbenzene-l,2-dithiol[38] in 10 mL of ether was added dropwise 2.2 mL (3.5 mmol) of 1.6 M BuLi in ether at 0 °C. The reaction mixture was allowed to warm to room temperature and was stirred for 1 h. Solvent was removed, the yellow residue was washed with ether and suspended in ether, and 0.7 mL (5.5 mmol) of Me_3SiCl was added. The mixture was stirred overnight and filtered. The filtrate was evaporated to afford the product as 360 mg (63%) of white solid. ^{1}H NMR ($CDCl_3$): δ 0.19 (s, 3), 2.21 (s, 1), 2.56 (s, 1).

Bis(1,2-trimethylsilylthio)-3,6-dichlorobenzene was prepared by the same procedure and isolated as a white solid. ^{1}H NMR: δ 0.16 (s, 9), 7.15 (s, 1).

$(Et_4N)_2[MO_3(Cl_2bdt)]$. a. M = W. To a solution of 51 mg (0.10 mmol) of $(Et_4N)_2[WO_4]$[39] in 5 mL of acetonitrile was added a solution of 21 mg (0.10 mmol) of $H_2(Cl_2bdt)$ in 5 mL of THF over 5 min. Solvents were removed, leaving a solid residue which was dissolved in 2 mL of acetonitrile. The solution was filtered. Addition of THF to the filtrate caused precipitation of a solid, which was collected and washed with THF to afford the product as 50 mg

(33) Wang, J.-J.; Groysman, S.; Lee, S. C.; Holm, R. H. *J. Am. Chem. Soc.* **2007**, 7512–7513.
(34) Lim, B. S.; Holm, R. H. *J. Am. Chem. Soc.* **2001**, *123*, 1920–1930.
(35) Jiang, J.; Holm, R. H. *Inorg. Chem.* **2005**, *44*, 1068–1072.
(36) Giolando, D. M.; Kirschbaum, K. *Synthesis* **1992**, 451–452.
(37) Herzog, U.; Böhme, U.; Rheinwald, G. *J. Organomet. Chem.* **2000**, *612*, 133–140.
(38) Schiødt, N. C.; Sommer-Larsen, P.; Bjornholm, T.; Nielsen, M. F.; Larsen, J.; Bechgaard, K. *Inorg. Chem.* **1995**, *34*, 3688–3694.
(39) Cotton, F. A.; Donahue, J. P.; Murillo, C. A. *Inorg. Chem.* **2001**, *40*, 2229–2233.
(40) McDonald, J. W.; Friesen, G. D.; Rosenhein, L. D.; Newton, W. E. *Inorg. Chim. Acta* **1983**, *72*, 205–210.

(71%) of a yellow solid. An analytical sample was recrystallized from acetonitrile/ether. IR: 908 (s), 845 (vs), 824 (vs) cm^{-1}. ^1H NMR: δ 6.74 (s). Anal. Calcd for $C_{22}H_{42}C1_2N_2O_3S_2W$: C, 37.67; H, 6.03; N, 3.99; S, 9.14. Found: C, 37.69; H, 6.52; N, 4.35; S, 9.65.

b. M = Mo. The same procedure on the same scale was employed but with use of $(Et_4N)_2[MoO_4]$ and an initial reaction temperature of −30 °C. The product was isolated as 31 mg (51%) of a red solid. IR: 883 (s), 842 (s), 824 (vs) cm^{-1}. ^1H NMR: δ 6.68 (s).

$(Et_4N)_2[WO_3(Me_4bdt)]$. A solution of 22 mg (0.063 mmol) of bis(1,2-trimethylsilylthio)tetramethylbenzene in 1 mL of THF was added dropwise to a solution of 32 mg (0.063 mmol) of $(Et_4N)_2[WO_4]$ in 2 mL of acetonitrile. The reaction mixture changed to yellow, solvent was removed, and the yellow-orange residue was washed with ether and THF. This material was crystallized from acetonitrile/ether at −28 °C to give the product as 21 mg (48%) of yellow crystals. IR: 912 (s), 839 (s), 812 (s) cm^{-1}. ES-MS: *m/z* 429 $(M + H)^-$. ^1H NMR: δ 2.37 (s, 1), 2.14 (s, 1).

$(Et_4N)_2[WO_2S(bdt)]$. Method A. This procedure has been briefly described;[33] a fuller account is given here. In a 20-mL container filled with dinitrogen, a light yellow solution of 128 mg (0.203 mmol) of $(Et_4N)_2[WO_3(bdt)]$[21] in 5 mL of acetonitrile was frozen at −78 °C. Gaseous H_2S was admitted to the headspace for 5 s. The temperature was raised to −30 °C, and the melted and well-stirred solution became bright orange. Volatiles were removed, leaving an orange-red solid residue which was washed with ether (−30 °C, 2 × 2 mL) and dissolved in 2 mL of acetonitrile. Ether (20 mL) was layered onto the solution. The solid that separated was collected and washed with ether to yield the product as 89 mg (68%) of deep orange plate-like crystals. Absorption, IR, and ^1H NMR spectral data and analytical data are given elsewhere.[33]

Method B. A solution of 73 mg (0.14 mmol) of $(Et_4N)_2[WO_3S]$[21] in 2 mL of acetonitrile at −30 °C was treated dropwise over 2 min with a solution of 36 mg (0.13 mmol) of 1,2-$C_6H_4(SSiMe_3)_2$ in 1 mL of THF at −30 °C. During the addition, the reaction mixture changed to red-brown. The mixture was allowed to warm to room temperature. Solvent was removed, and the brown residue was washed with ether and THF. It was dissolved in a mixture of 2 mL of acetonitrile and 1 mL of THF, and the solution was filtered. THF (2 mL) was added to the red filtrate, and the mixture was maintained at −30 °C. After 90 min, the mixture was filtered, 10 mL of ether was layered on the filtrate, and the mixture was allowed to stand at −30 °C overnight. The product was isolated as 55 mg (67%) of an orange crystalline solid. Absorption and ^1H NMR spectra are identical to those of the product of Method A.

$(Et_4N)_2[WO_2S(Cl_2bdt)]$. A solution of 30 mg (0.15 mmol) of $H_2(Cl_2bdt)$ was added dropwise to a solution of 70 mg (0.15 mmol) of $(Et_4N)_2[WO_3S]$ in 2 mL of acetonitrile. The addition was initiated at −30 °C, generating a deep orange color. As the addition proceeded, the reaction mixture was warmed to room temperature, and a precipitate formed. The mixture was filtered, and 10 mL of ether was layered onto the filtrate. The mixture was maintained at −30 °C for 2 h, resulting in the precipitation of a yellow-orange solid. This material was separated from the pale yellow solution, washed with ether, and recrystallized from acetonitrile/THF at −30 °C overnight. The product was isolated as 28 mg (27%) of an orange solid. IR: 906 (s), 825 (s), 447 (m), 426 (vs) cm^{-1}. Absorption spectrum: λ_{max} (ϵ_M) 334 (5300), 374 (2700) nm. ES-MS: *m/z* 459 $(M + H)^-$, 848 $(M + 3Et_4N)^+$. ^1H NMR: δ 6.79 (s).

$(Et_4N)_4[WO_2S(Me_4bdt)][WOS_2(Me_4bdt)]$. A solution of 30 mg (0.087 mmol) of 1,2-$C_6Me_4(SSiMe_3)_2$ in 1 mL of THF was added to dropwise to a solution of 50 mg (0.095 mmol) of $(Et_4N)_2[WO_3S]$ in 2 mL of acetonitrile at −30 °C. The yellow reaction mixture was allowed to warm to room temperature, during which time the color changed to deep red. Solvent was removed; the oily red residue was washed with ether and THF and dissolved in 2 mL of acetonitrile. The solution was filtered, and 3 mL of THF was added, causing precipitation of a red solid (18 mg). Red crystals were obtained by ether diffusion in a concentrated acetonitrile solution at −30 °C. ^1H NMR: δ 2.151 (1), 2.155 (1), 2.370 (1), 2.373 (1). The NMR spectrum and the X-ray crystal structure showed the solid to be an equimolar mixture of the title complexes. Attempts to prepare the individual complexes were unsuccessful.

$(Et_4N)_2[WOS_2(bdt)]$. A solution of 60 mg (0.11 mmol) of $(Et_4N)_2[WO_2S_2]$[40] was treated with 29 mg (0.10 mmol) of 1,2-$C_6H_4(SSiMe_3)$ in 1 mL of THF also at −30 °C. During the addition, the reaction mixture changed to dark brown. After the mixture warmed to room temperature, volatiles were removed, and the brown, sticky residue was washed with ether and THF. It was dissolved in a mixture of 2 mL of acetonitrile and 1 mL of THF, and the solution was filtered. Ether (10 mL) was layered onto the red filtrate, and the mixture was allowed to stand at −30 °C. The solid that separated was recrystallized from 2.7:1 THF/acetonitrile (v/v) to afford the product as 27 mg (41%) of red solid. IR: 446 (vs), 421 (s) cm^{-1}. Absorption spectrum: λ_{max} (ϵ_M) 263 (sh, 18 200), 338 (9000), 380 (sh, 2700), 481 (2500) nm. ES-MS: *m/z* 405 $(M + H)^-$. ^1H NMR: δ 6.63 (dd, 1), 7.12 (dd, 1). Anal. Calcd for $C_{22}H_{44}N_2OS_4W$: C, 39.75; H, 6.67; N, 4.21; S, 19.30. Found: C, 37.85; H, 6.74; N, 4.48; S, 19.69. Low carbon analyses were obtained on two samples.

$(Et_4N)_2[WOS_2(Cl_2bdt)]$. A solution of 36 mg (0.10 mmol) of bis(1,2-trimethylsilylthio)-3,6-dichlorobenzene in 3 mL of THF was added to a solution of 57 mg (0.11 mmol) of $(Et_4N)_2[WO_2S_2]$ in 2 mL of acetonitrile at −30 °C. The solution was stirred for 10 min, and solvent was removed to give dark red crystals, which were washed with ether to yield 60 mg (82%) of product. IR (KBr): 912 (s), 782 (m), 445 (s), 424 (m) cm^{-1}. Absorption spectrum: λ_{max} (ϵ_M) 294 (sh, 11 000), 330 (8190), 474 (3330) nm. ^1H NMR: δ 6.77. Anal. Calcd for $C_{22}H_{42}Cl_2N_2OS_4W$: C, 36.02; H, 5.77; N, 3.82; S, 17.48. Found: C, 36.70; H, 5.50; N, 3.46; S, 16.58.

$(Et_4N)_2[WOS_2(S_2C_2Me_2)]$. To an orange-brown solution of 25 mg (0.035 mmol) of $(Et_4N)_2[WO(S_2C_2Me_2)_2]$[41] in 2 mL of acetonitrile was added a solution of 19 mg (0.049 mmol) of Ph_3SbS in 2 mL of THF. Immediately after addition, the reaction mixture turned deep green, then green-blue, and after several minutes deep red. The mixture was stirred for 7 min, and 15 mL of ether was added. The red-brown oily solid that separated over 90 min was dried, giving 16 mg (50%) of product as a red solid. IR: 893 (s), 440 (s), 417 (s) cm^{-1}. Absorption spectrum: λ_{max} (ϵ_M) 263 (sh, 11 000), 338 (sh, 3450), 477 (2700), 675 (630) nm. ES-MS: *m/z* 382 (M^-). ^1H NMR: δ 1.95.

$(Et_4N)[WOS(OSiPh_3)(bdt)]$. Method A. At −20 °C, a solution of 16 mg (8.2 mmol) of Ph_3SiSH in 2 mL of acetonitrile was added to a solution of 31 mg (4.1 mmol) of $(Et_4N)[WO_2(OSiPh_3)(bdt)]$[21] in 5 mL of acetonitrile. The reaction mixture was allowed to warm to room temperature and was stirred for 10 min. Solvent was removed, and the residue was washed with ether (3 × 3 mL) and dissolved in 2 mL of acetonitrile. The solution was layered with 30 mL of ether and allowed to stand at −20 °C overnight. The solid was collected and washed with ether to afford the product as 21 mg (68%) of red-brown crystals. IR: 957, 922, 511 cm^{-1}. ES-MS: *m/z* 647 (M^-). Absorption spectrum: λ_{max} (ϵ_M) 300 (9950), 358 (sh, 4650), 461 (1000), 587 (370) nm. ^1H NMR: δ 6.87 (dd, 2), 7.21 (dd, 2), 7.43 (m, 9), 7.68 (m, 6). Anal. Calcd for $C_{32}H_{39}NO_2S_3SiW$: C, 49.42; H, 5.05; N, 1.80; S, 12.37. Found: C, 49.51; H, 5.12; N, 1.76; S, 12.42.

Method B. A solution of 30 mg (0.046 mmol) of $(Et_4N)_2[WO_2S(bdt)]$ in 2 mL of acetonitrile was treated with 10 mg (0.036 mmol) of Ph_3SiCl in 1 mL of THF. The reaction mixture changed from orange-red to brown and was stirred for 10 min. Solvent was removed, and the brown residue was washed with ether and extracted with THF/acetonitrile (7:1 v/v). Solvent was removed, and the solid was crystallized from acetonitrile/THF/ether at −30 °C, leading to 13 mg (46%) of product as a brown solid whose

(41) Goddard, C. A.; Holm, R. H. *Inorg. Chem.* **1999**, *38*, 5389–5398.

spectroscopic properties are identical with those of the product obtained with Method A.

(Et_4N)[WOS(OSiPr$^i_3$)(bdt)]. To a solution of 86 mg (0.13 mmol) of $(Et_4N)_2[WO_2(OSiPr^i_3)(bdt)]$[22] in 3 mL of THF was added 49 mg (0.26 mmol) of Pr^i_3SiSH in 3 mL of THF. The reaction mixture was stirred for 24 h, during which time the color changed from green to red-brown. Solvent was removed, and the residue was washed with ether to afford the product as 80 mg (91%) of a red-brown solid. ES-MS: *m*/*z* 545 (M^-). Absorption spectrum: λ_{max} (ϵ_M) 300 (6340), 350 (3320), 490 (310) nm. ^{1}H NMR: δ 1.15 (d, 18), 6.85 (dd, 2), 7.21 (dd, 2) (CH not detected).

(Et_4N)[WS_2($OSiPh_3$)(bdt)]. A solution of 36 mg (12.3 mmol) of Ph_3SiSH in 5 mL of acetonitrile was added to a solution of 31 mg (4.1 mmol) of $(Et_4N)[WO_2(OSiPh_3)(bdt)]$ in 10 mL of acetonitrile. The reaction mixture was stirred for 12 h, the solvent was removed, and the residue was washed with ether (3 × 3 mL). The dark red-brown solid was dissolved in 1.5 mL of acetonitrile, 30 mL of ether was layered onto the filtrate, and the mixture was maintained at −30 °C overnight. The brown crystalline solid was collected, washed with ether, and dried to afford 22 mg (68%) of product. IR: 946, 510, 471 cm^{-1}. ES-MS: *m*/*z* 663 (M^-). Absorption spectrum: λ_{max} (ϵ_M) 307 (11 900), 328 (sh, 7960), 365 (sh, 4170), 406 (sh, 2170), 473 (1320), 580 (370) nm. ^{1}H NMR (CD_3CN): δ 6.91 (dd, 2), 7.29 (dd, 2), 7.44 (m, 9), 7.71 (m, 6). Anal. Calcd for $C_{32}H_{39}NOS_4SiW$: C, 48.42; H, 4.95; N, 1.76; S, 16.16. Found: C, 48.24; H, 4.84; N, 1.72; S, 16.27.

(Et_4N)[WS_2($OSiPh_2Bu^t$)(bdt)]. To a solution of 25 mg (0.037 mmol) of $(Et_4N)_2[WOS_2(bdt)]$ in 2 mL of acetonitrile was added 10 mg (0.035 mmol) of Bu^tPh_2SiCl in 1 mL of THF, causing a color change from red-orange to dark brown. The reaction mixture was stirred for 10 min, solvent was removed, and the brown residue was washed with ether and extracted with 1 mL of THF. The extract was layered with 15 mL of ether, causing separation of a solid which was crystallized from acetonitrile/THF/ether at −30 °C to afford the product as 13 mg (50%) of brown solid. IR: 933 (s), 504 (s, br) cm^{-1}. Absorption spectrum: λ_{max} (ϵ_M) 307 (9400), 332 (6600), 426 (1700), 488 (sh, 870), 588 (300) nm. ^{1}H NMR: δ 1.13 (9), 6.90 (dd, 2), 7.28 (dd, 2), 7.42 (m 6), 7.88 (m, 4).

$(Et_4N)_2$[Mo_2O_2(μ_2-S)$_2$(bdt)$_2$]. In a 20-mL container filled with dinitrogen, a colorless solution of 110 mg (0.202 mmol) of $(Et_4N)_2[MoO_3(bdt)]$[21] in 5 mL of acetonitrile was frozen at −78 °C. Gaseous H_2S was admitted to the headspace for 5 s. The temperature was raised to 0 °C, the solid melted, and the well-stirred solution became red-brown. While the system was at 0 °C, volatiles were removed slowly, leaving a mixture of red-brown crystals and a green-brown, sticky material. The latter was removed by washing at 0 °C with acetonitrile/THF (3 × 10 mL, 3:1 v/v) and acetonitrile/ether (2 × 5 mL, 1:2 v/v), leaving red-brown, needle-like crystals which were dried to afford 66 mg (79%) of product. IR: 919 cm^{-1}. ES-MS: *m*/*z* 284 (M^{2-}). ^{1}H NMR: δ 6.93 (dd, 2), 7.53 (dd, 2). Anal. Calcd for $C_{28}H_{48}MoN_2O_2S_6$: C, 40.57; H, 5.84; N, 3.38; S, 23.21. Found: C, 40.43; H, 5.72; N, 3.45; S, 23.33.

X-ray Structure Determinations. Structures of the eight compounds in Table 1 were determined. In this section, for simplicity, compounds are designated by the numbers of their complexes given in Chart 1. Crystallographic data for **1** and **2**[21] and **8**, **14**, **15**, and **19**[33] have been previously reported. Diffraction-quality crystals of **11** were obtained by ether diffusion into an acetonitrile/DMF solution at room temperature; crystals of all other compounds were grown by ether diffusion into acetonitrile solutions at −30 °C. Crystal mounting and data collections were performed as described on a Siemens (Bruker) SMART CCD instrument using Mo Kα radiation.[10] Data out to 2θ of 50° were used for **3**, **4**, **10**/**13**, **11**, **12**, and **18** because of the somewhat lower quality of the high-angle data; for **5** and **17**, higher angle data were employed.

Data reductions were performed with SAINT, which corrects for Lorentz polarization and decay. Space groups were assigned by analysis of symmetry and systematic absences determined by

Table 1. Crystallographic Data[a] for Compounds Containing Molybdenum or Tungsten Oxo/Sulfido Benzenedithiolate Complexes

	$(Et_4N)_2$[**3**]	$(Et_4N)_2$[**4**]	$(Et_4N)_2$[**5**]	$(Et_4N)_4$[**10**][**13**]	$(Et_4N)_2$[**11**] · DMF[d]	$(Et_4N)_2$[**12**]	(Et_4N)[**17**]	(Et_4N)[**18**]
formula	$C_{22}H_{42}Cl_2MoN_2O_3S_2$	$C_{22}H_{42}Cl_2N_2O_3S_2W$	$C_{26}H_{52}N_2O_3S_2W$	$C_{26}H_{50}N_2O_{1.5}S_{3.5}W$	$C_{25}H_{51}N_3O_2S_4W$	$C_{22}H_{40}Cl_2N_2OS_4W$	$C_{32}H_{39}NOS_4SiW$	$C_{30}H_{43}NOS_4SiW$
fw	613.54	701.45	688.67	710.74	737.78	731.55	793.82	773.83
cryst syst	monoclinic	monoclinic	tetragonal	monoclinic	orthorhombic	orthorhombic	triclinic	triclinic
space group	*Cc*	*Cc*	$P4_3$	$P2_1/c$	$P2_12_12_1$	*Pbca*	$P\bar{1}$	$P\bar{1}$
Z	4	12	4	4	4	8	2	4
a, Å	13.2607(9)	16.093(2)	10.4760(2)	21.347(4)	11.0172(7)	13.9726(9)	9.2753(9)	10.1752(8)
b, Å	14.901(1)	40.136(5)	10.4760(2)	9.508(2)	14.7202(9)	14.3223(9)	9.950(1)	16.695(1)
c, Å	14.301(1)	13.999(2)	27.243(1)	16.045(3)	19.881(1)	29.797(2)	20.736(2)	21.702(2)
α, deg	90	90	90	90	90	90	79.190(2)	110.262(1)
β, deg	93.356(1)	111.896(2)	90	109.01(1)	90	90	88.356(2)	100.372(2)
γ, deg	90	90	90	90	90	90	64.132(1)	91.711(1)
V, A^3	2821.0(3)	8389.9(2)	2989.9(2)	3079.0(9)	3224.2(3)	5963.0(7)	1688.4(3)	3385.0(4)
d_{calcd}, g/cm^3	1.445	1.666	1.530	1.533	1.520	1.630	1.561	1.518
μ, mm^{-1}	0.827	4.496	4.031	4.012	3.867	4.351	3.729	3.718
2θ, deg	4.12−50.0	2.02−50.0	4.16−55.8	4.04−50.0	3.44−50.0	4.90−50.0	2.00−57.4	2.64−50.0
R_1[b] (wR_2[c])	0.0275 (0.0667)	0.0382 (0.0734)	0.0211 (0.0444)	0.0505 (0.0898)	0.0254 (0.0510)	0.0919 (0.2275)	0.0480 (0.1056)	0.0592 (0.1055)
GOF (F^2)	1.055	1.012	0.967	1.015	1.061	1.083	0.951	0.987

[a] Mo Kα radiation (λ = 0.71073 Å), 193(2) K. [b] $R_1 = \sum||F_o| - |F_c||/\sum|F_o|$. [c] $wR_2 = \{\sum[w(F_o^2 - F_c^2)^2]/(F_o^2)^2]\}^{1/2}$. [d] 188 K.

Chart 1. Designation of Complexes and Abbreviations

$[M^{VI}O_3(bdt)]^{2-}$	M = Mo, **1**; W, **2**[21]
$[M^{VI}O_3(Cl_2bdt)]^{2-}$	M = Mo, **3**; W, **4a−c**
$[W^{VI}O_3(Me_4bdt)]^{2-}$	**5**
$[W^{VI}O_2(OSiPr^i_3)(bdt)]^{-}$	**6**
$[W^{VI}O_2(OSiPh_3)(bdt)]^{-}$	**7**
$[W^{VI}O_2S(bdt)]^{2-}$	**8a,b**[33]
$[W^{VI}O_2S(Cl_2bdt)]^{2-}$	**9**
$[W^{VI}O_2S(Me_4bdt)]^{2-}$	**10**
$[W^{VI}OS_2(bdt)]^{2-}$	**11**
$[W^{VI}OS_2(Cl_2bdt)]^{2-}$	**12**
$[W^{VI}OS_2(Me_4bdt)]^{2-}$	**13**
$[W^{VI}OS_2(S_2C_2Me_2)]^{2-}$	**14a,b**[33]
$[W^{VI}OS(OSiPr^i_3)(bdt)]^{-}$	**15**[33]
$[W^{VI}OS(OSiPh_3)(bdt)]^{-}$	**16**
$[W^{VI}S_2(OSiPh_3)(bdt)]^{-}$	**17**
$[W^{VI}S_2(OSiPh_2Bu^t)(bdt)]^{-}$	**18a,b**
$[Mo^{V}_2O_2(\mu_2\text{-}S)_2(bdt)_2]^{2-}$	**19**[33]

AOR, aldehyde oxidoreductase; ap, apical; ba, basal; bdt, benzene-1,2-dithiolate(2−); Cl_2bdt, 3,6-dichlorobenzene-1,2-dithiolate(2−); DFT, density functional theory; DMSOR, dimethylsulfoxide reductase; Me_4bdt, 3,4,5,6-tetramethylbenzene-1,2-dithiolate(2−); Me_4phen, 3,4,7,8-tetramethyl-1,10-phenanthroline; QOR, quinoline 2-oxidoreductase; S_2pd, pyranopterindithiolate(2−); SP, square pyramidal; TBP, trigonal bipyramidal; XDH, xanthine dehydrogenase; XOR, xanthine oxidoreductase.

XPREP. Where appropriate, a choice of a space group was confirmed by PLATON. Structures were solved by direct methods and SHELXL-97 and refined against all data in the 2θ ranges by full-matrix least-squares on F^2. All non-hydrogen atoms were refined anisotropically except those indicated below. Hydrogen atoms at idealized positions were included in final refinements. Compounds **10** and **13** co-crystallized from the same reaction mixture in an equimolar ratio in the structure $(Et_4N)_4$[**10**][**13**], which refined satisfactorily with $^1/_2$O and $^1/_2$S at one basal ligand position. Compound **4** crystallized with three independent anions of distinct conformations in the asymmetric unit. Compound **18** has two nearly identical conformers in the asymmetric unit. One of the six independent cations in **4** and one of the two in **12** are disordered. They were modeled by two positions of equal occupancy and were described isotropically. Crystallographic data and final agreement factors are given in Table 1.[42]

Other Physical Measurements. All measurements were performed under anaerobic conditions. ^{1}H NMR spectra were recorded with a Bruker DMX-500 or Varian Mercury 300/400 spectrometer. Absorption spectra were obtained with a Varian Cary 50 Bio spectrophotometer, and infrared spectra with a Nicolet 5PC FT-IR instrument. Electrospray mass spectra were measured on acetonitrile solutions directly infused into an LCT mass spectrometer.

Computational Methods. Density functional calculations were performed using the Gaussian 03 (G03)[43] and Amsterdam Density Functional (ADF, versions 2004.01 and 2007.01)[44] software packages. G03 was used for calculations (molybdenum complexes only) involving the SVWN[45] local density approximation functional and the DGDZVP[46] double-ζ split-valence, singly polarized basis set. ADF calculations employed the BP86[47] general gradient approximation functional and the all-electron TZ2P[48] basis set (triple-ζ quality, doubly polarized Slater-type orbitals) with scalar relativistic (ZORA) corrections.[49]

Complexes were constrained to the highest symmetries where possible. Optimized geometries were verified as minima or transition states by frequency calculations. Default convergence criteria were used in all G03 calculations. For ADF calculations, the presence of low-frequency modes necessitated tight gradient and coordinate uncertainty criteria (10^{-4} hartree/Å and 10^{-3} Å, respectively) and higher numerical integration accuracy (evaluation to six significant digits) to yield accurate geometries for numerical frequency calculations; likewise, the integration accuracy for the frequency calculations was increased to eight digits. Solvent effects in acetonitrile were incorporated via the Conductor Polarizability Continuum Model (CPCM)[50] in G03 and the Conductor-like Screening Model (COSMO)[51] in ADF. Program defaults were used for the dielectric constant and molecular radius of acetonitrile (36.64 and 2.155 Å in G03, 37.5 and 2.76 Å in ADF). The PBE0/6-31G(d)-optimized UAKS United Atom Topological Model[52] provided the atomic radii for CPCM calculations; for COSMO calculations, the optimized radii of Klamt et al.[53] were employed where available; otherwise, the van der Waals radii of Bondi[54] were used, scaled by a factor of 1.2,[53] with the radius of the transition metal arbitrarily set to 2.4 Å.

Results and Discussion

The synthetic scheme affording structural analogues of the sites in the XOR family and related complexes is set out in Figure 2. The complexes were isolated as Et_4N^+ salts and divide into two sets: $[WO_{3-n}S_n(bdt)]^{2-}$ and their monosilylated derivatives $[WO_{2-n}S_n(OSiR_3)(bdt)]^-$. As in previous work on sulfite oxidase site analogues,[55] benzenedithiolate provides a plausible representation of the steric and electronic features of the pyranopterindithiolene cofactor ligand (Figure 1). 3,6-Dichlorobenzenethiolate and tetramethylbenzenedithiolate were employed in several cases to provide additional structural examples of a given molecular type. The use of tungsten in place of the native metal molybdenum is justified by numerous isostructural examples of d^0 complexes at parity of ligation.[56]

Synthesis of Complexes. a. $[WO_{3-n}S_n(bdt)]^{2-}$. The synthetic scheme originates with trioxo complexes **2**, **4**, and **5**, obtainable

(42) See additional data in the Supporting Information.
(43) Frisch, M. J.; et al. *Gaussian 03*, Revision C.02; Gaussian, Inc.: Wallingford, CT, 2004.
(44) (a) *ADF2007.0*; SCM, Theoretical Chemistry, Vrije Universiteit: Amsterdam, The Netherlands, 2006; http://www.scm.com. (b) te Velde, G.; Bickelhaupt, F. M.; van Gisbergen, S. J. A.; Fonseca Guerra, C.; Baerends, E. J.; Snijders, J. G.; Ziegler, T. *J. Comput. Chem.* **2001**, *22*, 931–967. (c) Fonseca Guerra, C.; Snijders, J. G.; te Velde, G.; Baerends, E. J. *Theor. Chem. Acc.* **1998**, *99*, 391–403.
(45) Slater exchange and VWN correlation functional III : 1517(a) Hohenberg, P.; Kohn, W. *Phys. Rev. B* **1964**, *136*, 864–871. (b) Kohn, W.; Sham, L. J. *Phys. Rev. A* **1965**, *140*, 1133–1138. (c) Slater, J. C. *Quantum Theory of Atoms and Molecules*; McGraw-Hill: New York, 1974; Vol. 4. (d) Vosko, S. H.; Wilk, L.; Nusair, M. *Can. J. Phys* **1980**, *58*, 1200–1210.
(46) (a) Godbout, N.; Salahub, D. R.; Andzelm, J.; Wimmer, E. *Can. J. Chem.* **1992**, *70*, 560–571. (b) Sosa, C.; Andzelm, J.; Elkin, B. C.; Wimmer, E.; Dobbs, K. D.; Dixon, D. A. *J. Phys. Chem.* **1992**, *96*, 6630–6636.
(47) (a) Becke, A. D. *Phys. Rev. A* **1988**, *38*, 3098–3100. (b) Perdew, J. P. *Phys. Rev. B* **1986**, *33*, 8822–8824; (erratum) Perdew, J. P. *Phys. Rev. B* **1986**, *34*, 7406 (c) The BP86 GGA correction is applied to the VWN (functional V) LDA functional, ref 45d.
(48) van Lenthe, E.; Baerends, E. J. *J. Comput. Chem.* **2003**, *24*, 1142–1156.
(49) (a) van Lenthe, E.; Baerends, E. J.; Snijders, J. G. *J. Chem. Phys.* **1993**, *99*, 4597–4610. van Lenthe, E.; Baerends, E. J.; Snijders, J. G. *J. Chem. Phys.* **1994**, *101*, 9783–9792. (b) van Lenthe, E.; Ehlers, E. J.; Baerends, E. J. *J. Chem. Phys.* **1999**, *110*, 8943–8953.
(50) (a) Barone, V.; Cossi, M. *J. Phys. Chem. A* **1992**, *102*, 1995–2001. (b) Cossi, M.; Rega, N.; Scalmani, G.; Barone, V. *J. Comput. Chem.* **2003**, *24*, 669–681.
(51) (a) Klamt, A.; Schüürmann, A. G. *J. Chem. Soc., Perkin Trans. 2* **1993**, 799. (b) Klamt, A. *J. Phys. Chem.* **1995**, *99*, 2224–2235. (c) Klamt, V.; Jones, J. *J. Chem. Phys.* **1996**, *105*, 9972–9981. (d) Pye, C. C.; Ziegler, T. *Theor. Chem. Acc.* **1999**, *101*, 396–408.
(52) Takano, Y.; Houk, K. N. *J. Chem. Theory Comput.* **2005**, *1*, 70–77.
(53) Klamt, V.; Jonas, T.; Burger, T.; Lohrenz, J. C. W. *J. Phys. Chem. A* **1998**, *102*, 5074–5085.
(54) Bondi, A. *J. Phys. Chem.* **1964**, *68*, 441–451.
(55) Lim, B. S.; Willer, M. W.; Miao, M.; Holm, R. H. *J. Am. Chem. Soc.* **2001**, *123*, 8343–8349.

by reaction of tungstate with 1,2-bis(trimethylsilylthio)benzene[21] or a dithiol. The original complexes of this type (**1**, **2**) were prepared by the first method and exhibit SP structures.[21] As will be seen, this stereochemistry, or distorted versions thereof, apply to all subsequently prepared species. From our recent report,[33] carefully controlled reaction of **2** with H_2S in acetonitrile at −30 °C, followed by addition of ether, affords the orange monosulfido complex **8** as the crystalline Et_4N^+ salt (68%). As an alternative to reaction 1, this complex may be obtained in essentially the same yield by the more convenient reaction 2, in which one reactant has the desired W═S bond in place. As a further example of this molecular type, the ring-substituted orange complex **9** was prepared by reaction 3, although in reduced yield (27%).

$$[WO_3(bdt)]^{2-} + H_2S \rightarrow [WO_2S(bdt)]^{2-} + H_2O \quad (1)$$

$$[WO_3S]^{2-} + 1,2\text{-}(Me_3Si)_2bdt \rightarrow [WO_2S(bdt)]^{2-} + (Me_3Si)_2O \quad (2)$$

$$[WO_3S]^{2-} + H_2(Cl_2bdt) \rightarrow [WO_2S(Cl_2bdt)]^{2-} + H_2O \quad (3)$$

Preparation of the $n = 1$ species **8** suggests the existence of $n = 2$ species. Red complex **11** is accessible by reaction 4 (41%), and the 3,6-dichloro complex **12** is obtained in an analogous manner (82%).

$$[WO_2S_2]^{2-} + 1,2\text{-}(Me_2Si)_2bdt \rightarrow [WOS_2(bdt)]^{2-} + (Me_3Si)_2O \quad (4)$$

Equimolar reaction 2, with 1,2-$(Me_3Si)_2Me_4$bdt, did give the desired $n = 1$ complex **10** which, however, crystallized with $n = 2$ complex **13** in a 1:1 ratio, evidently as a result of an undefined disproportionation reaction. The compound $(Et_4N)_4$[**10**][**13**] was used for structure determination and was not characterized further. Another example of an oxodisulfido species is the dimethyldithiolene complex **14**,[33] whose preparation is included in Figure 2. Because of its simple spectrum, the stability of **9** in acetonitrile (δ 6.79) was monitored by ^{1}H NMR. No appreciable decomposition was observed after 3 days at room temperature or after 3 h at 65 °C. In particular, the signals of **4** (δ 6.74) and **12** (δ 6.77) did not appear, indicating the absence of a disproportionation reaction.

b. $[WO_{2-n}S_n(OSiR_3)(bdt)]^-$. Silylation of terminal W═O bonds has limited precedent, among them the group transformations $W^{VI}O_3 \rightarrow W^{VI}O_2(OSiR_3)$[21,22,57,58] and $W^{IV}O \rightarrow W^{IV}(OSiR_3)$.[58] Trioxo complex **2** is readily silylated to yield **6** and **7**,[21,22] which are sulfidated in reaction 5 by silylthiols (R = Pr^i, Ph) to afford the desired $n = 1$ oxosulfido complexes **15** (91%) and **16** (46−68%). Direct silylation reaction 6 provides an example of the $W^{VI}O_2S \rightarrow W^{VI}OS(OSiR_3)$ conversion, affording **16** (46%). The use of additional equivalents of thiol in reaction 5 leads to the $n = 2$ disulfido species **17** (68%). The related complex **18** (50%) was obtained from **11** by the transformation $W^{VI}OS_2 \rightarrow W^{VI}S_2(OSiR_3)$. This work provides additional examples of the utility of silylthiols, particularly (commerically available) Ph_3SiSH,[21,22] in M═O → M═S conversions. Donahue[59] has provided an extensive tabulation of other sulfur transfer reagents.

$$[WO_2(OSiR_3)(bdt)]^- + nR_3SiSH \rightarrow [WO_{2-n}S_n(OSiR_3)(bdt)]^- + nR_3SiOH \quad (5)$$

$$[WO_2S(bdt)]^{2-} + Ph_3SiCl \rightarrow [WOS(OSiPh_3)(bdt)]^- + Cl^- \quad (6)$$

Absorption Spectra. The different sulfide content in the complexes $[WO_{3-n}S_n(bdt)]^{2-}$ and $[WO_{2-n}S_n(OSiR_3)(bdt)]^-$ are clearly reflected in the absorption spectra of Figure 3. In the first set, solution colors more obviously differ: $n = 0$ (**2**, yellow), 1 (**8**, orange), 2 (**11**, red). In both sets, complexes with $n = 1$ and $n = 2$ manifest bands in the visible region, which are shifted to lower energy in the order $n = 2 > 1$, while those with $n = 0$ absorb only in the UV region. The strong feature at 481 nm for **8** (474 nm for **12**) is indicative of the $n = 2$ composition and is useful for detecting this impurity in the preparation of $n = 1$ complexes. Visible bands are ligand-to-metal charge-transfer (LMCT) transitions implicating sulfido ligands, whereas those of $n = 0$ complexes are likely LMCT involving the oxo and/or bdt ligand(s). We do not presently have a basis for a detailed spectral interpretation. Progressive shifts of LMCT bands like those observed here have also been found for the series $[MoO_{3-n}S_n(OSiPr^i_3)]^-$ ($n = 0-3$)[22] and $[MO_{2-n}S_n(OSiPh_3)_2(Me_4phen)]$ (M = Mo, W; $n = 0-2$).[24,30]

Stereochemistry. X-ray structures have been determined for selected examples of the preceding two sets of complexes as Et_4N^+ salts. These are of three general types, the large majority of which approach SP stereochemistry with bdt always in a basal position. Under this arrangement, the complexes $[MX_3(bdt)]$ (C_s), $[MX_2Y(bdt)]$ ($C_1 + C_s$), and $[MXYZ(bdt)]$ ($3C_1$) have 0, 2, and 3 possible diastereomers, respectively, arising from different ligands in the apical position. Structures are depicted in Figures 4−7. Metric data for the basis set of complexes $[W^{VI}O_{3-n}S_n(bdt)]^{2-}$ ($n = 0-2$) included in Table 2; data for other complexes are available elswehere.[42]

a. Shape Parameters. The stereochemistry of five-coordinate molecules has been analyzed in some detail,[60−62] and shape parameters have been proposed to distinguish square pyramidal (SP) and trigonal bipyramidal (TBP) forms which, in general, are interconvertible via a low-energy Berry pseudorotation. The term "square pyramidal" is used in the vernacular inasmuch as the basal unit of such SP molecules considered here is certainly not square. For molecules [MOXY(bdt)] with one bidentate and three unidentate ligands, we describe molecular shapes in terms of the five parameters defined in Figure 8, where X and Y are oxo and/or sulfido ligands. While all parameters can be calculated for any shape, the perpendicular metal displacement δ and the dihedral angle θ in particular are most easily visualized as descriptors for SP stereochemistry, as in previous reports of tungsten dithiolene complexes.[63−65] The distance parameter ϵ measures the position of the metal atom from the OXY plane, while the parameters φ and previously introduced τ[62] convey

(56) In past reports, we have made the more general statement that isoelectronic isoligated molybdenum and tungsten molecules are isostructural. Recently, Kuiper et al. have demonstrated that a pair of four-coordinate d^2 complexes have different spin ground states and are not isostructural (Kuiper, D. S.; Douthwaite, R. E.; Mayol, A.; Wolczanski, P. T.; Lobkovsky, E. B.; Cundari, T. R.; Lam, O. P.; Meyer, K. *Inorg. Chem.* **2008**, *47*, 7139–7153). No such behavior is expected, or has been observed, for d^0 complexes of these elements.

(57) Partyka, D. V.; Staples, R. J.; Holm, R. H. *Inorg. Chem.* **2003**, *42*, 7877–7886.

(58) Lorber, C.; Donahue, J. P.; Goddard, C. A.; Nordlander, E.; Holm, R. H. *J. Am. Chem. Soc.* **1998**, *120*, 8102–8112.

(59) Donahue, J. P. *Chem. Rev.* **2006**, *106*, 4747–4783.

(60) Muetterties, E. L.; Guggenberger, L. J. *J. Am. Chem. Soc.* **1974**, *96*, 1748–1756.

(61) Favas, M. C.; Kepert, D. L. *Prog. Inorg. Chem.* **1980**, *27*, 325–463.

(62) Addison, A. W.; Nageswara Rao, T.; Reedijk, J.; van Rijn, J.; Verschoor, G. C. *J. Chem. Soc., Dalton Trans.* **1984**, 1349–1356.

(63) Sung, K.-M.; Holm, R. H. *Inorg. Chem.* **2000**, *39*, 1275–1281.

(64) Sung, K.-M.; Holm, R. H. *J. Am. Chem. Soc.* **2001**, *123*, 1931–1943.

(65) Sung, K.-M.; Holm, R. H. *Inorg. Chem.* **2001**, *40*, 4518–4525.

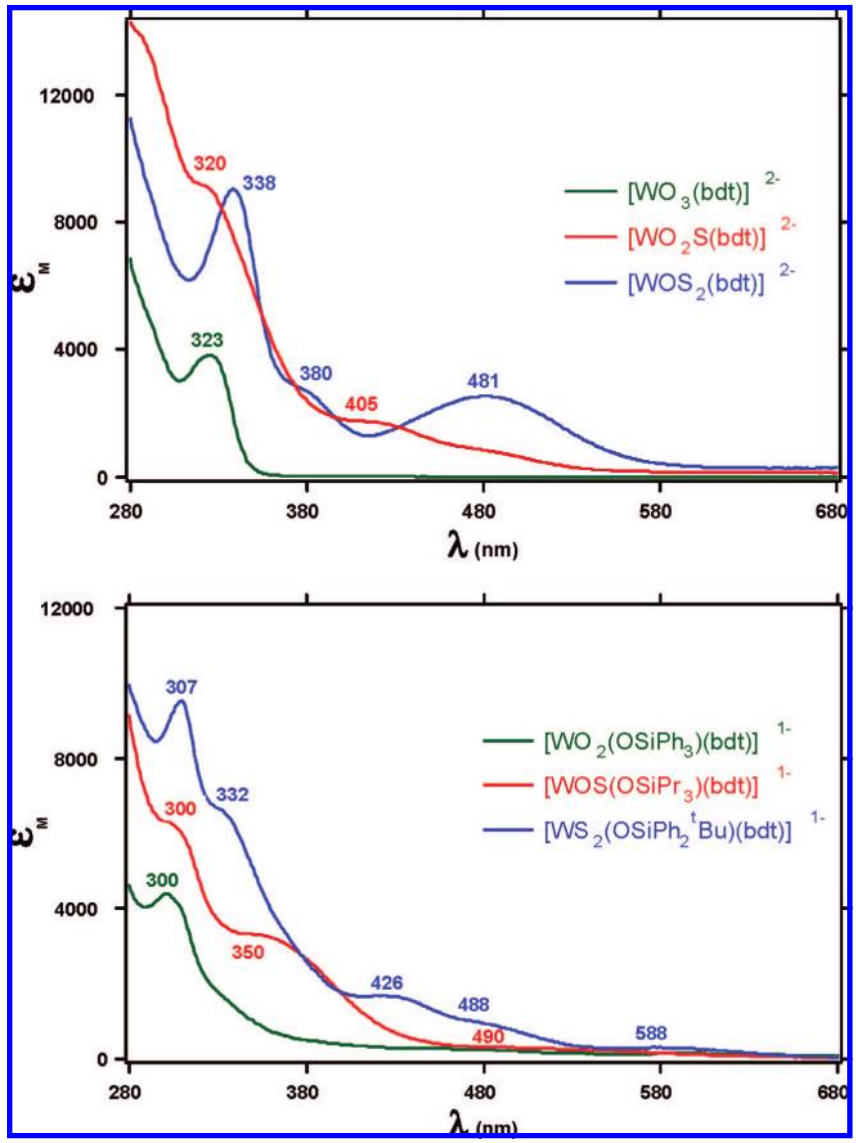

Figure 3. UV−visible absorption spectra of $[WO_{3-n}S_n(bdt)]^{2-}$ ($n = 0-2$ (**2**, **8**, **11**), upper) and $[WO_{2-n}S_n(OSiR_3)(bdt)]^{-}$ ($n = 0-2$ (**7**, **15**, **18**), lower) in acetonitrile solutions. Absorption maxima are indicated.

overall molecular shape. The parameter τ is defined as $(\alpha - \beta)/60$, where α and β are the largest and next-largest interligand bond angles, respectively. For idealized SP geometry $\tau = 0$, and for idealized TBP geometry $\tau = 1$.

For DFT calculations, we employ an additional conformational parameter φ defined as the dihedral angle $S_1-ft-M-X$, where X is the unique chalcogenide (if present; X = O for MO_3 and MOS_2 groups, S for MO_2S), ft is the perpendicular foot of the MS_1S_2 triangle, and S_1 is a fixed bdt atom. The parameter φ can be viewed as a measure of the rotation of the pyramidal MOXY group[66] relative to the MS_1S_2 chelate plane. This parameter does not set the positions of O and Y, and therefore, the φ value by itself does not directly equate to a coordination stereochemistry. Nevertheless, if the MOXY group is treated as an approximate three-fold rotor relative to the chelate plane, we expect that, within the unique range of $\varphi = 0-90°$ for MO_2S and MOS_2, SP structures will correlate with φ values near 30° and 90° and TBP geometries with φ values near 0° and 60°. For MO_3 species, we correlate an SP structure with $\varphi = 30°$ and 90°. Experimental and computational structures confirm these relationships.

Shape parameters are collected in Table 3 for 16 complexes and three protein sites. We note the common features of dihedral angles $\theta = 125-137°$, tungsten atom displacements $\delta = 0.54-0.62$ Å from the SSXY basal mean plane, and positions $\epsilon = 0.67-0.82$ Å from the OXY face of the coordination unit, with the larger values of the latter associated with X = Y = S. Note also the structural variability and different conformational forms (**a**−**c**) of certain complexes in their crystalline Et_4N^+ salts.

b. $[WO_{3-n}S_n(bdt)]^{2-}$. The structures of trioxo complexes **3**−**5** have been determined; shape parameters are tabulated for **1**−**5**. Complexes **1**, **2**, **3**, and **5** approach the SP limit. Crystals of $(Et_4N)_2$[**4**] contain three independent anions, **4a**−**c**, which differ markedly in conformation (Figure 4). Complex **4a** is essentially SP, whereas **4b** and **4c** are progressively displaced from this limit, as is evident from the rotational positions of the WO_3

(66) Trans influence is a significant stereochemical and metric factor for d^0 complexes with terminal oxo and/or sulfido ligands. We know of no examples in which these ligands orient trans to each other in such molecules.

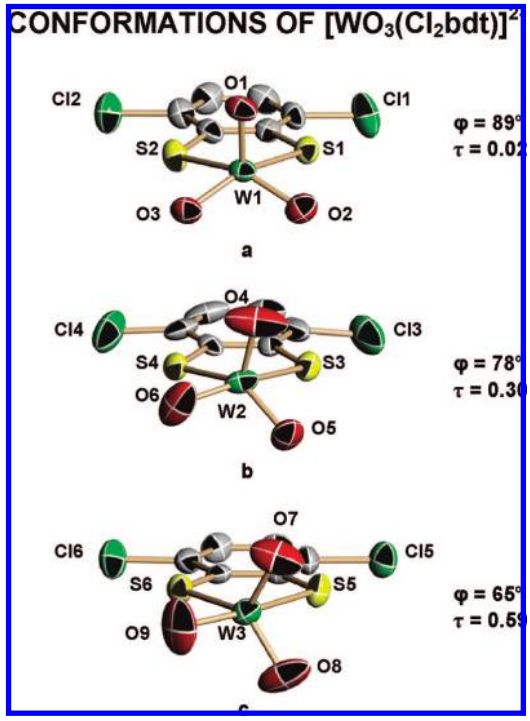

Figure 4. Conformations of the three independent anions in crystalline $(Et_4N)_2[WO_3(Cl_2bdt)]$ (**4a**−**c**) with 50% thermal ellipsoids and atom labeling schemes; values of the shape parameters φ and τ are indicated. Selected bond distances (Å): **4a**, mean W1−O 1.76(2), W1−S1 2.543(2), W1−S2 2.518(2); **4b**, W2−O4 1.781(7), W2−O6 1.768(7), W2−S3 2.578(2), W2−S4 2.493(2); **4c**, mean W3−O 1.74(1), W3−S5 2.588(2), W3−S6 2.485(2).

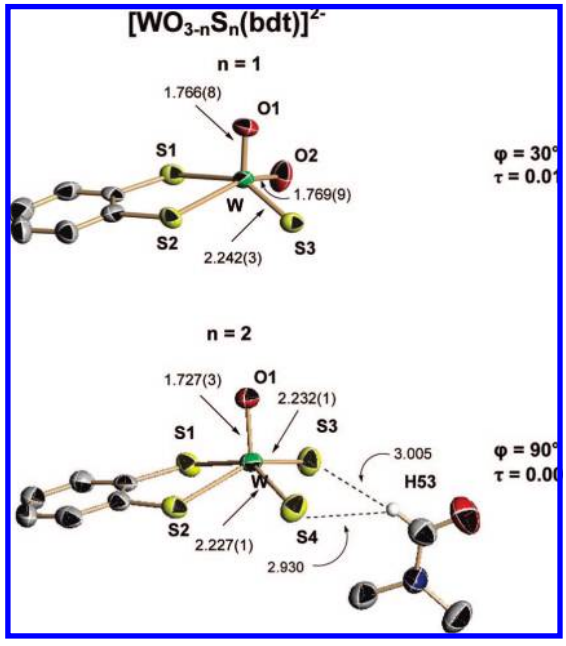

Figure 5. Structures of $[WO_{3-n}S_n(bdt)]^{2-}$ (n = 1 (**8a**), 2 (**11**)). with 50% thermal ellipsoids, atom labeling schemes, selected bond distances (Å), and shape parameters φ and τ. A DMF solvate molecule is hydrogen-bonded to **11**.

group relative to the chelate plane. Indeed, **4c** exhibits the largest τ value in the MO_3 set and the smallest φ value of any complex examined (Table 3) and approaches the TBP limit. Accompanying these distortions are changes in W−O bond lengths and apical-basal bond angles and larger differences in trans-basal

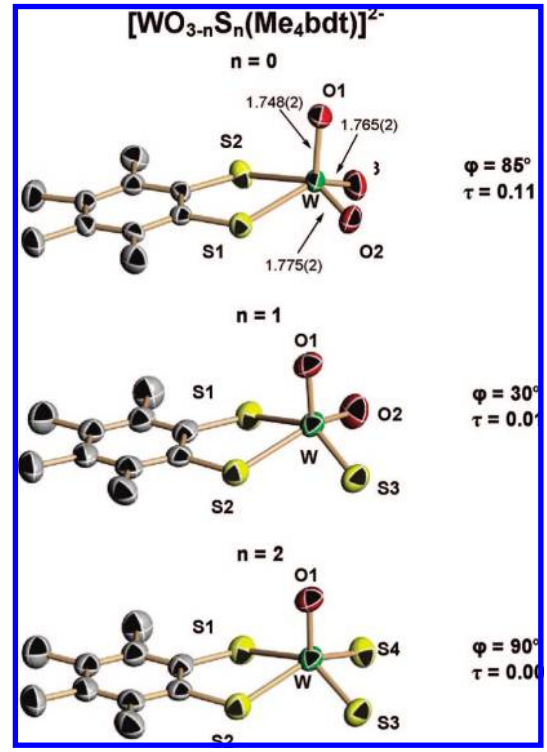

Figure 6. Structures of $[WO_{3-n}S_n(Me_4bdt)]^{2-}$ (n = 0−2 (**5**, **10**, **13**)) with 50% thermal ellipsoids, atom labeling schemes, selected bond distances (Å), and shape parameters φ and τ.

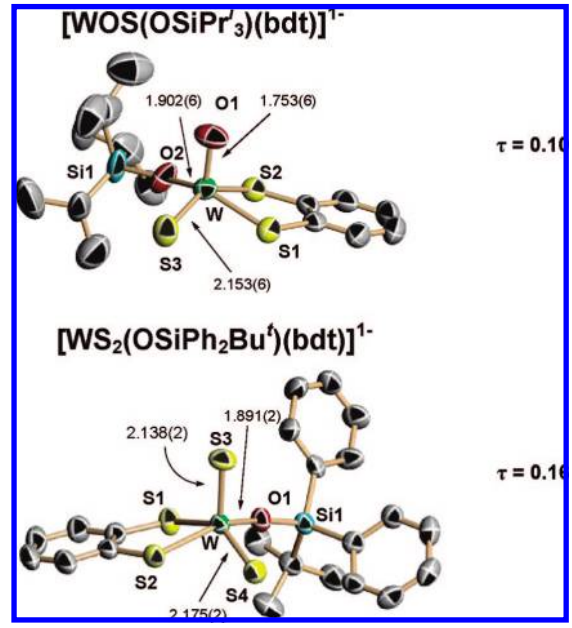

Figure 7. Structures of silyloxide complexes $[WOS(OSiPr^i_3)(bdt)]^-$ (**15**, upper) and $[WS_2(OSiPh_2Bu^t)(bdt)]^-$ (**18a**, lower) with 50% thermal ellipsoids, atom labeling schemes, selected bond distances (Å), and τ parameters.

angles relative to **4a**. In **4a**, atoms O2 and O3 are approximately coplanar with and directly opposite to S2 and S1, respectively, with nearly equal S−W−O basal (trans) angles. Consequently, O2 and O3 impose a comparable trans influence on the bonds W1−S2 and W1−S1, which differ in length by 0.025 Å. In **4b,c**, one oxo ligand (O6, O9) is placed in a similarly opposite location to a sulfur atom with larger basal angles. This results

Table 2. Bond Distances (Å) and Angles (deg) in the Series $[WO_{3-n}S_n(bdt)]^{2-}$, $n = 0, 1, 2$

	$n = 0$[a]	$n = 1$[b]	$n = 2$
W−O1	1.752(2)	1.766(8)	1.727(3)
W−O2	1.744(2)	1.768(9)	
W−O3	1.769(2)		
W−S1	2.521(1)	2.467(3)	2.470(1)
W−S2	2.538(1)	2.514(3)	2.482(1)
W−S3		2.243(3)	2.227(1)
W−S4			2.232(1)
	apical-basal		
O1−W−S1	106.5(1)	104.4(3)	104.2(1)
O1−W−S2	101.9(1)	104.6(3)	104.5(1)
O1−W−O2	107.2(1)	106.2(5)	
O1−W−O3	106.2(1)		
O1−W−S3		106.3(3)	106.7(1)
O1−W−S4			106.5(1)
	basal-basal		
S1−W−S2	77.75(4)	78.7(1)	78.62(4)
S1−W−O2	80.28(8)	80.8(3)	
S2−W−O3	81.75(7)		
S2−W−S3		81.7(1)	81.07(4)
O2−W−S3		102.2(3)	
S1−W−S4			81.29(4)
O2−W−O3	103.6(1)		
S3−W−S4			102.08(5)
	trans-basal		
S1−W−O3	143.4(1)		
S2−W−O2	148.4(1)	146.3(4)	
S1−W−S3		146.8(1)	146.33(4)
S2−W−S4			146.27(5)

[a] Reference 21. [b] A second independent non-disordered anion has very similar dimensions.

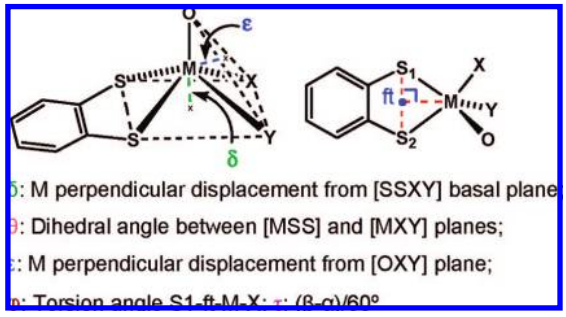

Figure 8. Definition of the shape parameters δ, θ, ϵ, τ, and φ (see text).

in enhanced differences in W−S bond lengths, amounting to 0.085 (**4b**) and 0.103 Å (**4c**), owing to a more pronounced trans influence of one oxo ligand. While we cannot specify the exact origins of the overall distortions or the causes of the more regular structure of Mo^{VI} complex **3**, the conformational variability of **4a**−**c** suggests a shallow potential energy surface for these and other d^0 complexes in this work.

Two dioxosulfido complexes have been structurally defined. Complex **8** is found in two nearly identical conformations which contain a *basal* sulfido ligand and apical and basal oxo ligands and closely approach the SP limit.[33] This stereochemistry also applies to **10**, which co-crystallized in the lattice of $(Et_4N)_4$[**10**][**13**] and was not isolated separately. Complexes **8** and **10** are the first synthetic species with the same basic stereochemistry as active sites in the XOR family. Oxodisulfido complexes **11** and **13** exhibit nearly perfect SP stereochemistry, and **12** is slightly deformed from this configuration. In these species, the oxo ligand occupies the apical position, leading to an SP structure with a S_4 basal plane. In addition, the dimethyldithiolene complex **14** occurs in two conformations, both displaced from SP geometry and depicted elsewhere.[33] The configuration of conformer **14b** resembles that of **4c** (see Table 5, below) and is severely disarranged from an SP structure.

Table 3. Shape Parameters for Five-Coordinate (bdt)MOXY

complex/site			δ (Å)	θ (°)	ϵ (Å)	φ (°)	τ[a]
$[MoO_3(bdt)]^{2-}$ [b]	**1**		0.542	134	0.676	86	0.08
$[WO_3(bdt)]^{2-}$ [b]	**2**		0.544	134	0.693	86	0.08
$[MoO_3(Cl_2bdt)]^{2-}$	**3**		0.543	134	0.671	84	0.13
$[WO_3(Cl_2bdt)]^{2-}$	**4**	**a**	0.553	134	0.684	89	0.02
		b	0.564	130	0.681	78	0.30
		c	0.565	125	0.681	65	0.59
$[WO_3(Me_4bdt)]^{2-}$	**5**		0.550	133	0.707	85	0.11
$[WO_2S(bdt)]^{2-}$	**8**	**a**	0.583	135	0.761	30	0.01
		b	0.583	134	0.767	28	0.05
$[WO_2S(Me_4bdt)]^{2-}$	**10**		0.625	135	0.811	30	0.01
$[WOS_2(bdt)]^{2-}$	**11**		0.628	134	0.806	90	0.00
$[WOS_2(Cl_2bdt)]^{2-}$	**12**		0.567	138	0.816	84	0.08
$[WOS_2(Me_4bdt)]^{2-}$	**13**		0.544	137	0.737	90	0.00
$[WOS_2(S_2C_2Me_2)]^{2-}$	**14**	**a**	0.619	134	0.795	84	0.15
		b	0.615	123	0.796	56	0.52
$MoO_2(OSiPh_2Bu^t)(bdt)]^{-}$ [c]			0.562	132			0.17
$[WO_2(OSiPr^i_3)(bdt)]^{-}$ [c]	**6**	**a**	0.568	131			0.24
		b	0.571	128			0.35
$[WOS(OSiPr^i_3)(bdt)]^{-}$	**15**		0.591	134			0.10
$[WS_2(OSiPh_2Bu^t)(bdt)]^{-}$	**17**	**a**	0.623	132			0.16
		b	0.621	131			0.19
$[WS_2(OSiPh_3)(bdt)]^{-}$	**16**		0.618	132			0.10
D. gigas AOR[d] (inactive)			0.601	133			0.02
P. putida QOR[e]			0.490	145	0.905	43	0.18
bovine milk XDH[f]			0.595	134			0.24

[a] Reference 62. [b] Reference 21. [c] Reference 22. [d] Reference 12. [e] Reference 19. [f] Reference 74.

Table 4. Computed Relative Energies[a] (kcal/mol) for Selected $[MO_{3-n}S_n(bdt)]^{2-}$ Stationary Points

	M = Mo		M = W
	SVWN/DGDZVP	BP86/TZ2P	BP86/TZ2P
	$[MO_3(bdt)]^{2-}$		
O_{ap}	0	0	0
$TS^{‡}$	0.4[b]	0.7	0.8
	$[MO_2S(bdt)]^{2-}$		
O_{ap}	0	0	0
S_{ap}	1.7	1.3	1.2
$TS^{‡}$	1.5[c]	1.9	1.8
	$[MOS_2(bdt)]^{2-}$		
O_{ap}	0	0	0
S_{ap}	1.0	1.2	1.3
$TS^{‡}$	0.8[c]	1.4	1.6

[a] Including zero-point correction and acetonitrile solvation (using CPCM for SVWN or COSMO for BP86). [b] The TBP geometry ($TS^{‡}$) is a local minimum at the SVWN/DGDZVP level. [c] The unphysical ordering of the SVWN $TS^{‡}$ and S_{ap} energies originates from the inclusion of nonelectrostatic solvation terms to the total energy.

Structures of two members, **8** and **11**, of the bdt series and three members of the Me_4bdt series **5**, **10**, and **13** are provided in Figures 5 and 6, respectively. Metric parameters for the bdt series including trioxo complex **2** are collected in Table 2. The W=O and W=S bond distances, while ca. 0.02−0.10 Å longer than sometimes encountered, are unexceptional. The $W-S_{bdt}$ bond lengths differ little (0.01−0.05 Å) because each molecule is at or near the SP limit, such that differential trans influences of ligands are reduced. These results demonstrate that, in these five-coordinate complexes, the intrinsic stereochemical preference is for an SP structure with one or two sulfido ligands in basal positions. The MOS_2 group has not been detected in any enzyme structure.

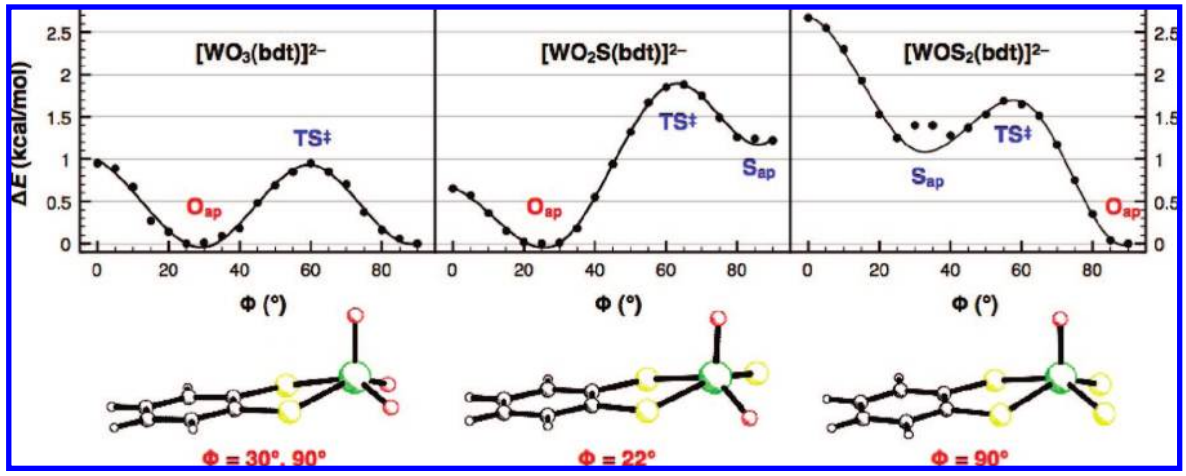

Figure 9. Energies of $[WO_{3-n}S_n(bdt)]^{2-}$ conformers as a function of the angle $\varphi = 0-90°$. Optimized, lowest energy structures and their φ values are shown below the corresponding plots. The potential energy curves represent cubic splines fitted to the electronic energies (BP86/TZ2P with CPCM solvation) of geometries optimized at fixed φ values. The irregular features at $\varphi = 30-35°$ in the $n = 2$ plot appear to be artifacts in the solvation model and were excluded from the spline fit. These features are absent in gas-phase calculations.[42]

c. $[WO_{2-n}S_n(OSiR_3)(bdt)]^-$. While certain trioxo molybdenum and tungsten complexes can be monoprotonated and the products isolated,[57,67−69] a similar result upon attempted protonation of sulfido complexes in general has not been obtained. Consequently, we have turned to silylation as a simulator of protonation. Structures of oxosulfido complex **15**,[33] and disulfido complexes **17** and **18**, which occur in two nearly identical conformations, have been determined. The latter two are isostructural; only the results for **18a** are presented (Figure 7).[42] All complexes are distorted from the SP limit. Complex **15** adopts a configuration with an apical oxo and basal silyloxo and sulfido ligation. In complex **18**, the apical position is occupied by a sulfido ligand. Structural differences between these two complexes are those that might be expected upon replacing an oxo with the larger sulfido ligand. The W═S distances in **15** and **18** are 0.07−0.11 Å shorter than in **8** and **10**−**14**, presumably because the former contain one fewer π-donor ligand. The configuration of **15**, and by implication **16** (for which diffraction-quality crystals were not obtained), is analogous to enzyme active sites with a basal hydroxo or aquo ligand (Figure 1). However, it cannot be claimed that this experimental stereochemistry is necessarily intrinsic because of the steric effects associated with bulky substituents.

Computational Analysis of Stereochemistry. The stereochemistry of $[MO_{3-n}S_n(bdt)]^{2-}$ complexes (M = Mo, W; $n = 0-2$) and their monoprotonated/monosilylated derivatives was investigated by DFT calculations. Two methods were used for detailed analysis, the SVWN functional in conjunction with the double-ζ DGDZVP basis set originally optimized for this functional, and the BP86 functional with a triple-ζ quality STO basis set (TZ2P) and relativistic corrections. The SVWN/DGDZVP combination is little used but was explored here because of its unexpected accuracy in replicating structural metrics in our systems (vide infra). Interestingly, the simpler SVWN/DGDZVP approach also gives energy descriptions for stereochemical rearrangements that are entirely comparable to those obtained from the presumably higher accuracy BP86/TZ2P treatment. We have found similar behavior in a recent study of oxo transfer thermodynamics involving molybenum complexes.[70] The SVWN/DGDZVP calculations were applied to molybdenum systems only, as the basis set is undefined for tungsten. The structural and energetic descriptions of analogous molybdenum and tungsten systems from the BP86/TZ2P calculations were essentially indistinguishable.

a. $[MO_{3-n}S_n(bdt)]^{2-}$. These complexes (M = Mo, W) show positive HOMO energies and negative vertical ionization potentials at all DFT levels surveyed, indicating that computational gas-phase models are unstable to electron autodetachment. Dielectric continuum solvation models (CPCM or COSMO) simulating acetonitrile solvation were therefore employed to construct more realistic descriptions of the complexes. Experimental solvation energies for dianions are scarce, and we are unaware of any attempts to calibrate continuum solvation models against them; accordingly, the accuracy of solvation treatments in the current context should be considered with caution.

The energies and interconversions of the various five-coordinate geometries were analyzed computationally via the distortion parameter φ. The energy profiles obtained from geometry optimizations at fixed values of φ, shown in Figure 9, reveal Berry pseudorotation pathways for each complex, connecting SP minima via TBP maxima. Frequency calculations at fully optimized geometries derived from these profiles confirm SP geometries as minima, whereas TBP geometries always represent, with the exception of **1** at the SVWN/DGDZVP level (Table 4), transition states for pseudorotation.

The relative energies of SP molecules and the TBP transition states that interconvert them are summarized in Table 4. Apical oxo SP geometries are consistently more stable than apical sulfido SP diastereoisomers. The energy differences are small throughout, with the relative energies, including those of transition states, spanning a range of less than 2 kcal/mol in all cases. The errors associated with the DFT energies are certainly greater than this for these systems, and quantitative accuracy cannot be expected. Nevertheless, the calculated results agree with experiment for monosulfido and disulfido complexes in

(67) Schreiber, P.; Wieghardt, K.; Nuber, B.; Weiss, J. *Z. Anorg. Allg. Chem.* **1990**, *587*, 174–192.
(68) Schreiber, P.; Wieghardt, K.; Nuber, B.; Weiss, J. *Polyhedron* **1989**, *8*, 1675–1682.
(69) Eagle, A. A.; George, G. N.; Tiekink, E. R. T.; Young, C. G. *Inorg. Chem.* **1997**, *36*, 472–479.
(70) Lee, S. C.; Holm, R. H. *Inorg. Chim. Acta* **2008**, *361*, 1166–1176.

Table 5. Comparative Metrics (Å) for $[MO_{3-n}S_n(bdt)]^{2-}$ Structures ($n = 0-2$)[a]

		terminal chalcogenide, M−Q			M−S_{bdt}	
method	M	M−O_{ap}	M−O_{ba}	M−S_{ba}	trans to O_{ba}	trans to S_{ba}
			$[MO_3(bdt)]^{2-}$			
experiment[b]	Mo	1.73	1.75, 1.76		2.54, 2.56	
	W	1.75	1.77, 1.78		2.52, 2.54	
SVWN/DGDZVP	Mo	1.76	1.78		2.51, 2.52	
BP86/TZ2P[c]	Mo	1.76	1.77		2.56	
	W	1.77	1.79		2.55	
			$[MO_2S(bdt)]^{2-}$			
experiment[d]	W	1.76	1.77	2.25	2.50	2.48
SVWN/DGDZVP	Mo	1.76	1.77	2.25	2.49	2.51
BP86/TZ2P	Mo	1.74	1.76	2.27	2.51	2.54
	W	1.76	1.77	2.27	2.51	2.53
			$[MOS_2(bdt)]^{2-}$			
experiment[d]	W	1.73		2.23, 2.23		2.47, 2.48
SVWN/DGDZVP	Mo	1.75		2.23, 2.24		2.48, 2.49
BP86/TZ2P[c]	Mo	1.73		2.25		2.50
	W	1.74		2.25		2.50
			$[MO_3(bdt)]^{2-}$, TBP geometry[e]			
		M−O_{ax}	M−O_{eq}		S_{ax}	S_{eq}
experiment[f]	W	1.75	1.73, 1.73		2.59	2.49
SVWN/DGDZVP	Mo	1.78	1.77, 1.77		2.57	2.48
BP86/TZ2P	Mo	1.77	1.76, 1.76		2.65	2.50
	W	1.79	1.77, 1.78		2.63	2.50

[a] DFT calculations include acetonitrile solvation (using CPCM for SVWN or COSMO for BP86) and are not symmetry-constrained unless otherwise indicated. [b] Reference 21. [c] C_s symmetry. [d] This work. [e] The $[MO_3(bdt)]^{2-}$ TBP geometry is a minimum at the SVWN level but a transition state in BP86 calculations. [f] This work, using distances from Cl_2bdt-ligated **4c**.

that (i) apical oxo SP geometries are found without exception in the crystalline state (Figures 5 and 6); (ii) approximate TBP structures similar to those computed as solution transition states are also occasionally found (Figure 4), implying that the TBP-type geometries can be accessed by relatively small energy perturbations (e.g., packing forces); and (iii) ^{1}H NMR solution studies reveal that the bdt ligand is in a symmetric environment down to −50 °C (vide infra), which is consistent with stereochemical fluxionality and low-energy barriers to polytopal rearrangement. Given that our comparisons involve relative energies of varying d^0 geometries, the computational stability rankings and magnitudes in energies appear feasible despite the relatively small energies involved. The minor differences in stability between apical oxo and apical sulfido isomers lead to the expectation that the latter should be isolable given a favorable lattice environment.

Theoretical treatments of the XOR oxidized active site, with the majority focused on reaction mechanism, have depicted distorted SP or TBP geometries,[71,72] sometimes without explicit comment. Bray and Deeth[71] concluded that apical oxo and apical sulfido forms are about equally stable; energetics data were not given.

(71) (a) Bray, M. R.; Deeth, R. J. *Inorg. Chem.* **1996**, *35*, 5720–5724. (b) Bray, M. R.; Deeth, R. J. *J. Chem. Soc., Dalton Trans.* **1997**, 1267–1268.

(72) (a) Voityuk, A. A.; Albert, K.; Huber, R.; Nasluzov, V. A.; Neyman, K. M.; Romão, M. J.; Rösch, N. *J. Am. Chem. Soc.* **1997**, *119*, 3159–3160. (b) Voityuk, A. A.; Albert, K.; Romão, M. J.; Huber, R.; Rösch, N. *Inorg. Chem.* **1998**, *37*, 176–180. (c) Illich, P.; Hille, R. *J. Phys. Chem. B* **1999**, *103*, 5406–5412. (d) Zhang, X.-H.; Wu, Y.-D. *Inorg. Chem.* **2005**, *44*, 1466–1471. (e) Bayse, C. A. *Inorg. Chem.* **2006**, *45*, 2199–2202. (f) Amano, T.; Ochi, T.; Sato, H.; Sakaki, S. *J. Am. Chem. Soc.* **2007**, *129*, 8131–8138.

Table 6. Computed Relative Energies[a] (kcal/mol) for Isomers of Monoprotonated $[MO_2S(bdt)]^{2-}$ (M = Mo, W)

	M = Mo		M = W
geometry	SVWN/DGDZVP	BP86/TZ2P	BP86/TZ2P
	$[MO_2(SH)(bdt)]^-$		
O_{ap}, syn	5.6	0.3	0.2
O_{ap}, anti	5.6	0	0
	$[MOS(OH)(bdt)]^-$		
O_{ap}, syn	0	0.1	0.3
O_{ap}, anti	2.5	2.1	1.9
S_{ap}, syn	0.5	0.7	0.7
S_{ap}, anti	2.8	2.6	2.3

[a] Referenced to the minimum energy geometry in each tautomeric set; includes zero-point correction and acetonitrile solvation (using CPCM for SVWN or COSMO for BP86).

Optimized structures compare well with the crystallographic determinations, as summarized in Table 5. For SP minima, calculated metal−ligand bond lengths are within 0.02 Å of experimental values. The largest variances are associated with M−S_{bdt} bonds, which are subject to the trans influence of oxo/sulfido ligands; these specific bond lengths are especially exaggerated in gas-phase calculations. The SVWN/DGDZVP method yields particularly accurate predictions for metal−ligand bond lengths. Superimposed fits of crystallographic and calculated structures (not shown) reveal that the largest deviations in overall geometry originate from bending distortions of the bdt chelate ring due, presumably, to solid-state packing.

The computed TBP structures reproduce the general trends found in the TBP structure of **4c** (Figure 4), although at lower accuracy relative to the SP results. The exaggerated thermal ellipsoids of **4c** suggest the presence of dynamic or static disorder along the low-energy pseudorotation pathway, due perhaps to the metastable nature of the TBP geometry. The discrepancies between calculated and experimental W−O bond lengths could be an artifact of this disorder, as the nature of the motion would serve to decrease the observed distances.

b. Protonated/Silylated $[MO_{3-n}S_n(bdt)]^{2-}$. Monoprotonation of these complexes at terminal oxo or sulfido sites adds the issues of OH/SH tautomerism and the rotational orientation of these groups to the stereochemical analysis. Geometry preferences were initially assayed by two-dimensional relaxed potential energy surface scans using as conformational parameters φ and S_{bdt}−M−(O/S)−H dihedral angles. Gas-phase SVWN/DGDZVP calculations were used in these surveys because the monoanions, unlike their dianion parents, were found to be computationally stable to electron autodetachment in the gas phase. Approximate local minima from these scans were fully optimized at the SVWN/DGDZVP and BP86/TZ2P levels using continuum solvation models to allow comparison with the dianion calculations. The relative energies of tautomeric species and conformers of protonated $[MO_2S(bdt)]^{2-}$, the case of principal biological interest (Figure 1), are summarized in Table 6. We note the following observations, which apply to the full set of protonated species whose relative energies are given elsewhere.[42]

(i) As in the dianion calculations, minima are always associated with SP geometries and, where the possibility exists for a given tautomer, the apical oxo diastereomer is more stable than the apical sulfido form, although energetic preferences are modest. Apical OH/SH geometries are not found to be minima, in keeping with the strong trans influence of terminal oxo or sulfido ligation.

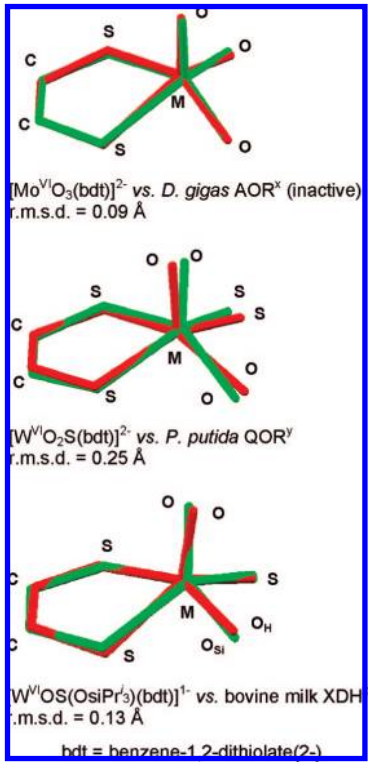

Figure 10. Best-fit superpositions of the indicated pairs of analogue (green) and enzyme site (red) structures: upper, **1** and inactive AOR; middle, **8a** and QOR; lower, **15** and XDH. X-ray structural data for the enzymes were taken from the Protein Data Bank. Fits were performed using OFIT in the SHELXS package and are expressed in terms of rmsd's in atom positions.

(ii) Ligands OH/SH adopt two possible conformations, with the hydrogen atom directed either toward the nearest S_{bdt} atom (syn) or ca. 180° opposed (anti). For the hydroxo ligand, the syn conformation is the more stable and appears to originate from a favorable internal electrostatic interaction between the polar O−H group and the trans-influenced S_{bdt} atom; this stabilization is significant (ca. 2 kcal/mol) relative to the other factors under consideration. The hydrosulfide ligand, by contrast, shows a smaller and inconsistent preference for hydrogen atom orientation that may arise from weaker polarization of the S−H group and the longer M−SH bond, which moves the hydrogen farther from interaction with other ligand atoms.

(iii) The SVWN/DGDZVP and BP86/TZ2P methods disagree on the most stable OH/SH tautomer. The SVWN results favor protonation at oxo, whereas the BP86 calculations show no energy preference that can be clearly disentangled from the influence of metal stereochemistry and OH/SH conformation. This difference represents the only situation in our study where the two methods diverge significantly in their predictions.

In the absence of protonated synthetic species, we consider the silylated monoanions **15** and **18** (Figure 8) against computational models optimized from initial crystallographic coordinates. The DFT structures of these complexes are slightly less accurate than those of the parent dianions, with metal−ligand bonds deviating from experiment by ca. 0.02−0.04 Å. The coordination geometries are otherwise reproduced, although the rotational orientations of the hindered silyl groups differ considerably because of crystal packing. Thus, **15** has apical oxo and basal sulfido and silyloxo ligands, and **18** has apical and basal sulfido and basal silyloxo. Calculated DFT energies for the pairs $[MOS(OSiMe_3)(bdt)]^-/[MO_2(SSiMe_3)(bdt)]^-$ and $[MS_2(OSiMe_3)(bdt)]^-/[MOS(SSiMe_3)(bdt)]^-$ (using the crystal structures of **15** and **18** as approximate starting geometries for optimization) predict that the O-silylated species are more stable than S-silylated forms by ca. 10 kcal/mol in both the SVWN/DGDZVP and BP86/TZ2P approaches. These results are consistent with the silylation behavior of oxosulfido molybdenum and tungsten complexes,[22,24,30] where the substantial difference in Si−O and Si−S bond energies (25−40 kcal/mol)[73] appears to dictate the more stable form.

Fluxionality. The ^{1}H NMR spectra of all complexes **1**−**18** in acetonitrile solutions at room temperature are consistent with static or dynamic structures in which ligands exhibit vertical mirror symmetry. For example, trioxo **2** (δ 7.07, 6.54), oxodisulfido **11** (δ 7.12, 6.63), and dioxosulfido **8** (δ 7.03, 6.56) show a pair of doublets of doublets (dd). For **2** and **11**, this is the expected result for SP species with static C_s symmetry. Three complexes were examined at 223−293 K in CD_3CN/THF-d_8 solvent mixtures. Over this range, **4** exhibited a sharp singlet and **11** an equally sharp doublet of doublets, a behavior attributed to SP structures equivalent to those observed in the solid state (Figures 4 and 5). One of the dd features of **8** gradually broadened as the temperature was decreased, but the slow exchange limit was not reached. This behavior, together with the two dd spectra of silyloxide complexes **15**−**18**, whose solid-state structures lack symmetry (Figure 7), indicates that the complexes are fluxional. The four inequivalent bdt protons can be equilibrated to equivalent pairs by attainment of a TBP-like transition state of low energy, as suggested by DFT calculations.

Comparison of Analogue and Protein Site Structures. Bond distances in the coordination spheres of analogues and oxidized protein sites (Figure 1) are in generally good agreement, but the estimated standard deviations of protein values are usually not quoted. For example, the mean Mo−S_{bdt} (2.54(1) Å) and Mo═O (1.75(1) Å) distances in **1**[21] are close to the values for an inactive (desulfo) form of *D. gigas* AOR.[12] The W−S_{bdt} (2.49(3) Å), mean W═O (1.767(1) Å), and W═S (2.243(3) Å) bond lengths of **8** conform moderately well with EXAFS data for bovine milk XOR at pH 10.[20] Further, the W−S_{bdt} (2.44(3) Å), W═O (1.753(1) Å), W═S (2.153(3) Å), and W−O_{Si} (1.902(6) Å) bond lengths of **15** approach or match those of the monoprotonated XOR site at pH 6.

The similarity of overall shapes of analogues and oxidized protein sites can be assessed from shape parameters (Table 3) and calculations of best-fit superimposed X-ray structures set out in Figure 10. Three pairs of structures were selected: **1** or **6** and the (mono)protonated inactive *D. gigas* AOR site (1.28 Å resolution),[12] **8a,b** and the dioxosulfido *P. putida* QOR site (1.8 Å resolution),[19] and **15** and the (presumably) monoprotonated bovine milk XDH site (2.0 Å resolution).[74] The fits are expressed in terms of root-mean-square deviations (rmsd's) in atom positions. The AOR site has normal shape values for SP stereochemistry, is nearly congruent with trioxo **1**, and is less closely related to silylated **6** and $[MoO_2(OSiPh_2Bu^t)(bdt)]^-$, both of which depart considerably from SP according to the τ criterion. The dioxosulfido QOR site and the XDH site are both

(73) (a) Luo, Y. R. *Handbook of Bond Dissociation Energies in Organic Compounds*; CRC Press: New York, 2003; pp 287−299. (b) Basch, H. *Inorg. Chim. Acta* **1996**, *252*, 265–279. (c) Leroy, G.; Temsamani, D. R.; Wilante, C. *J. Mol. Struct.* **1994**, *306*, 21–39.
(74) Fukunari, A.; Okamoto, K.; Nishino, T.; Eger, B. T.; Pai, E. F.; Kamezawa, M.; Yamada, I.; Kato, N. *J. Pharmacol. Exp. Ther.* **2004**, *311*, 519–528.

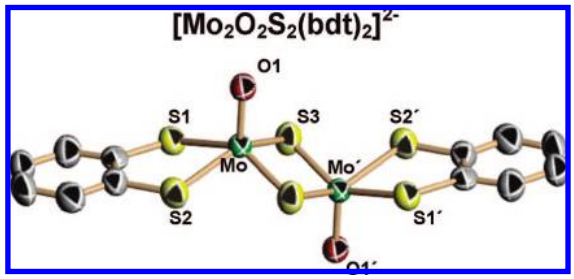

Figure 11. Structure of centrosymmetric $[Mo_2O_2S_2(bdt)_2]^{2-}$ with 50% probability ellipsoids and the atom labeling scheme. Selected bond lengths (Å) and angles (deg): mean Mo−S_{bdt} 2.408(9), Mo−O 1.687(6), mean Mo−(μ_2-S) 2.308(1), Mo−Mo 2.902(1), Mo−(μ_2-S)−Mo 77.91(8), (μ_2-S)−Mo−(μ_2-S) 102.09(8).

further displaced from the SP limit than are **8a,b** and **15**, respectively. The fit of **8a** and QOR gives the largest rmsd, as is visually evident from Figure 8, but is still rather good. The metric comparisons and superimposed structure fits, while differing in precision, demonstrate that molecules of the types $[MO_3(bdt)]^{2-}$ (M = Mo, W), $[WO_2S(bdt)]^{2-}$, and $[WOS(OSiR_3)(bdt)]^-$ are credible structural analogues of inactive and active enzyme sites, respectively, in the XOR family.

Molybdenum vs Tungsten Stability. We have encountered a number of instances in which the Mo^{VI} analogues of tungsten−sulfur compounds are unstable in a reducing sulfur ligand environment and could not be isolated. Examples include $[MoO_2(S_2C_2R_2)_2]^{2-}$, $[MoO(OR)(S_2C_2R_2)]^{2-}$, $[MoQ(SR)(S_2C_2R_2)]^-$ (R = alkyl, Ph; Q = O, S), and now $[MoO_2S(bdt)]^2$. As recently reported,[33] attempted formation of the last complex under the same conditions used for the preparation of **8** from **2** and H_2S afforded the Et_4N^+ salt of the binuclear Mo^V complex **19** (79%). We have not established the stoichiometry of the reaction, but the likely reductant is H_2S. The identity of the product was established by the X-ray structure in Figure 11. The $[Mo_2O_2(\mu_2\text{-}S)_2]^{2+}$ core contains a planar Mo_2S_2 portion and transoid oxo ligands. Dinuclear complexes of this type are precedented,[75,76] including $[Mo_2O_2S_2(S_2C_2H_4)_2]^{2-}$ in which, however, the oxo ligands are cisoid.[75] The present result notwithstanding, certain Mo^{VI} oxo-dithiolene complexes are stable to isolation, including **1**,[21] $[MoO_2(bdt)_2]^{2-}$,[77] and $[MoO(OSiR_3)(bdt)_2]^-$.[78]

Summary

This and previous work[21,22,33] has resulted in the synthesis of two series of monodithiolene complexes, $[M^{VI}O_{3-n}S_n(bdt)]^{2-}$ and their silylated derivatives $[M^{VI}O_{2-n}S_n(OSiR_3)(bdt)]^-$ (n = 0, M = Mo or W; n = 1 or 2, M = W), that form the basis of the structural analogue chemistry in the XOR enzyme family. The large majority of complexes approach or achieve SP stereochemistry, while others are deformed from this arrangement by solid-state interactions. The species $[MO_3(bdt)]^{2-}$ and $[MO_2(OSiR_3)(bdt)]^-$, with a basal silyloxo group, represent unprotonated and monoprotonated sites, respectively, of inactive enzymes. The monosulfido species $[WO_2S(bdt)]^{2-}$ and $[WOS(OSiR_3)(bdt)]^-$, with apical oxo and basal sulfido and silyloxo ligands, are the first analogues of unprotonated and protonated catalytic sites, respectively. Disulfido complexes possess two basal sulfido ligands or one apical sulfido and one basal silyloxo ligand. DFT calculations predict minimum energy SP structures that, in general, correspond to those observed in crystalline Et_4N^+ salts. Although the energy differences between SP and TBP structures and SP diasteromeric forms of a given complex as predicted by DFT calculations are small, the minimum energy structures correspond in all cases to those observed in crystalline Et_4N^+ salts. For example, the correct structure is predicted for $[WO_2S(bdt)]^{2-}$, whose basal and apical sulfido diastereomers are potentially interconvertible through a low-lying TBP transition state for pseudorotation. The lowest energy tautomer of the protonated form is calculated to be $[WOS(OH)(bdt)]^-$, in which the hydroxo ligand is basal with a syn orientation of the O−H proton toward a S_{bdt} atom. These collective results of calculated and observed structures suggest that protein sites adopt intrinsic coordination geometries rather than those dictated by protein structure and environment.

Acknowledgment. This research was supported at Harvard University by NSF Grant CHE 00547734 and by NSERC at the University of Waterloo. We thank Dr. M. Nooijien (Waterloo) and SHARCNET (www.sharcnet.ca) for access to computational resources, and Prof. P. T. Wolczanski for the information in footnote 56 prior to publication.

Supporting Information Available: X-ray crystallographic files in CIF format for the eight compounds in Table 1; tabulated metric data for complexes **5**, **15**, and **18**; plots of computed gas-phase relative energies of $[MoO_{3-n}S_n(bdt)]^{2-}$ (n = 0−2) as a function of φ; computed solution-phase relative energies for the protonated forms of complexes $[MO_{3-n}S_n(bdt)]^{2-}$ (M = Mo, W; n = 0−2); complete ref 43. This material is available free of charge via the Internet at http://pubs.acs.org.

JA804000K

(75) Hsieh, T.-C.; Gebreyes, K.; Zubieta, J. *Transition Met. Chem.* **1985**, *10*, 81–84.
(76) Coucouvanis, D. *Adv. Inorg. Chem.* **1997**, *45*, 1–73.
(77) Ueyama, N.; Oku, H.; Kondo, M.; Okamura, T.; Yoshinaga, N.; Nakamura, A. *Inorg. Chem.* **1996**, *35*, 643–650.
(78) Donahue, J. P.; Goldsmith, C. R.; Nadiminti, U.; Holm, R. H. *J. Am. Chem. Soc.* **1998**, *120*, 12869–12881.